To Improve Axial Compressive Behavior of Concrete Filled Double Skin Tubular (CFDST) Short Column

A Thesis of

Master of Science

By

Luqman Ali

(NUST-2019-MS SE 00000320208)

Submitted to

Dr. Hassan Sagheer

September 2023

Department of Structural Engineering

Military College of Engineering, Risalpur

National University of Science & Technology

Islamabad, Pakistan

THESIS ACCEPTANCE CERTIFICATE

This is to certify that the

thesis titled

To Improve Axial Compressive Behavior of Concrete Filled Double Skin Tubular (CFDST) Short Column

Submitted by

Luqman Ali

(00000320208)

has been accepted towards the partial fulfillment

of the requirements for the degree of

Master of Science in Structural Engineering

Dr. Hassan Sagheer

Assistant Professor,

Department of Structural Engineering,

Military College of Engineering, Risalpur

National University of Sciences and Technology (NUST), Islamabad

ii

DECLARATION

I certify that this research work titled "**To Improve Axial Compressive Behavior of Concrete Filled Double Skin Tubular (CFDST) Short Column**" is my own work. The work has not been presented elsewhere for assessment. The material that has been used from other sources it has been properly acknowledged / referred.

Signature of Student

Luqman Ali

(2018-NUST-MS SE-00000320208)

iii

Plagiarism Certificate (Turnitin Report)

This thesis has undergone a plagiarism check, and a Turnitin report approved by my supervisor is attached for reference.

Signature of Student

Luqman Ali

NUST-2019-00000320208-MCE

Signature of Supervisor

Dr. Hassan Sagheer

This thesis is dedicated to my family.

ACKNOWLEDGEMENTS

ABSTRACT

Concrete filled double skin tubular (CFDST) are promising members in recent decades which was proven to be a competitive structural member compared to traditional steel tubular members. It provides an efficient composite action between steel and concrete. Concrete filled double-skin tubular has been studied for its strength and ductility. This research aims to experimentally investigate the compressive behavior of circular concrete filled double-skin steel tubular (CFDST) short columns, in which both the sandwiched concrete and steel tube is under axial compression. For this purpose, Steel tubes of two different diameter one of larger diameter and other of smaller diameter were used with high strength concrete sand-witched between them. Total 8 specimens were prepared in the study and their axial load-shortening curves, ultimate strength and failure modes were briefly discussed. Two sample were prepared for the comparison of concrete filled double skin tubular column having no shear studs with the column having shear studs on the inner face of outer steel tube and the outer face of inner steel tube. For strengthening the strategic location of outer steel tube. In the first series, we're starting with the outer steel tube having wall thickness of 1mm. In 2nd series we've taken different approaches for strengthening of outer steel tube. This strengthening has been applied at various strategic locations. Such as top mid and bottom. In series 3 the entire thickness of steel tube increase to 2 mm. At the end we have to compare series-2 sample with series1 and series3. Result suggest that Shear studs significantly enhance load-carrying capacity in C-SC columns compared to C-WSC. Shear studs reduce susceptibility to sudden failures from local buckling o instability. Bonding strength and prevention of local buckling are key roles of shear studs in CFDST columns. With the increase of the wall thickness and yield stress at critical area of outer steel tube, the failure mode of the specimens gradually changes from diagonal shear failure to axial compression failure. The CFDST short column having extra strengthening on the outer steel tube increase the maximum load carrying capacity from 10 to 20% with respect to the control mix. The load-carrying capacity increases as the confinement of the outer steel tube increase due to the larger confining pressure provided to the infilled concrete.

TABLE OF CONTENTS

LIST OF FIGURES

LIST OF TABLES

LIST OF ABBREVIATIONS

HSC   High Strength Concrete

CFST   Concrete Filled Steel Tubular

CFDST   Concrete Filled Double Skin Tubular

NSC   Normal Strength Concrete

HSLWC   High Strength Light Weight Concrete

LWC   Light Weight Concrete

LFC   Light Foamed Concrete

LWA   Light Weight Aggregate

SCMs   Self-Compacting Mortars

GGBFS   Ground Granulated Blast Furnace Slag

NS   Nano silica

SF   Silica Fume

FA   Fly Ash

TC   Thermocouples

LVDTs   Linear Variable Displacement Transducers

INTRODUCTION

1.1 Introduction

A concrete-filled double-skin tubular (CFDST) column is a structural element composed of two concentric steel tubes filled with concrete. Typically, the outer steel tube has a circular or rectangular shape, while the inner tube is circular. Concrete is placed in the space between the inner and outer tubes, and it acts as the main component for carrying loads in the column.

CFDST columns offer several advantages over traditional reinforced concrete columns, such as improved structural strength, ductility, and durability. The use of steel tubes in the design provides additional stiffness and buckling resistance, while the concrete filling provides enhanced compressive strength.

These types of columns are commonly used in high-rise building construction and are particularly suitable for tall and slender structures. The design of CFDST columns can be customized to meet specific project requirements, such as varying column heights and load capacities. CFDST columns are also resistant to seismic activity, making them an excellent choice for buildings located in earthquake-prone areas.

1.2 Significance of Research

Fully concrete filled steel tubes (CFST) have seen a significant growth in utilization in recent years. The structural performance of CFST are better compared to those made of steel or non - reinforced concrete. The tubes of the CFST column act as formwork and work as reinforcement for concrete. Due to steel hollow section the local buckling of concrete eliminated or delayed, and increase section ductility. Construction using CFST technology has proven to be economical in terms of materials and time, resulting in further cost reductions.

In composite construction, the benefits of both steel and concrete are integrated. The primary benefits include quick construction, high strength, steel's light weight, concrete's inherent mass, damping. Compared to bare reinforced concrete or bare steel, they function

structurally better. Construction using the CFDST method has shown to be economical in terms of materials and time, resulting in further cost reductions.

Columns made of concrete-filled steel tubes are widely used in the construction industry due to their favorable ratio of cross-sectional area to load-carrying capacity, this kind of structural elements are actually preferred in practice. Thus, smaller pieces of CFDST columns can be used in place of the larger massive concrete columns seen in the lowest floors of tall buildings. Additionally, CFDST components can serve as bridge piers in crowded places. Therefore, such structural components must to be carefully examined before being used in important constructions. The behavior of CFST and CFDST columns under various loading conditions has been a subject of research for approximately 50 years, but it remains incompletely understood. Therefore, comprehensive parametric studies are essential to gain a full understanding of CFDST column behavior.

1.3 Background

For more than a century, steel-concrete composite columns were used. It was initially utilized to protect steel constructions from fire. The design then took into account the strength characteristics of the concrete-encased columns. However, the 1960s marks the beginning of research into concrete filled steel tubes (CFST). [1]

Nowadays tall buildings, bridges, and other structures increasingly use composite structural components. Due to its composite properties, the advantages and disadvantages of two materials can be combined to create a structural system that is effective. Steel and concrete composites are an efficient way to carry significant axial. The steel portion to withstand any shear forces, tensile forces and bending moments strengthens the concrete. Along with resisting compressive loading, in a composite column, the concrete reduces the chance that the steel portion may buckle.

Compared to conventional reinforced concrete columns required to support the same load, the usage of composite columns whether encased or infilled reduces the column size significantly. As a result, significant financial savings are possible. Additionally, where floor space is limited, like in office buildings and parking lots, the column size reduction is favorable. Additionally, the tabular idea allows for the high-rise buildings' use of sparsely

spaced composite columns joined to spandrel beams on their exteriors to withstand lateral stresses. [1]

Many seismic resistant structures prefer concrete-encased steel composite components. The section becomes less rigid when the concrete encasing fractures due to severe flexural overloading, but the steel core still offers ductile resistance and shear capacity to successive cycles of stress. Furthermore, the concrete cover has preserved the surface area of the encased steel parts, negating the need for painting and fireproofing expenses. For many high-rise building columns including earthquake-resistant constructions, bridge piers, concrete filled double steel tube CFDST columns are preferred. If the structure needs to be protected against fire, additional fire-resistant insulation is required for the concrete-filled steel tubes. Because of steel tubes may be utilized as scaffolding, the CFDST constructions can be built more easily.

1.4   Concrete Filled Double Skin Tube (CFDST)

1.4.1   Shape of CFDST

Geometry of the confining steel tube, double-skinned, concrete-filled steel tubes come in various shapes, including rectangular, circular, L-shaped, square, elliptical, etc. Circular section and square sections are the most commonly used shapes in construction for CFDSTs. When subjected to a static load, circular CFDST columns exhibit strain-hardening or elastic-perfectly-plastic behavior after yielding. In contrast, the load-deformation curve for hollow structural steel columns deteriorates after yielding under the same loading conditions.
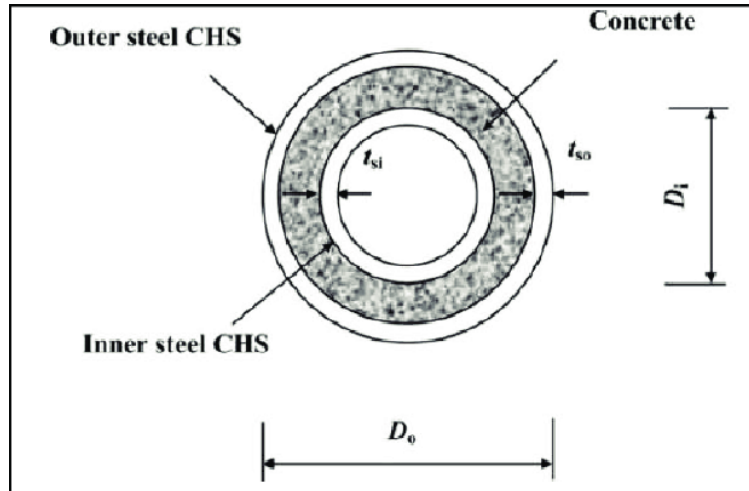
Figure 1. 1 Cross Section of Circular CFDST Column

1.4.2 Behavior during loading

Concrete infill and steel of the CFDST column will experience longitudinal deformation during the first phases of concentric axial loading. Naturally, it is anticipated that the CFDST segment will experience homogeneous concentric loading. At these starting strains, the structural steel's Poisson's ratio (approximately 0.28) is greater than that of infill concrete, which ranges 0.15 to 0.25. As a result, along the column, there is localized separation between the two composite components. Additionally, there is little to no contact between these two materials. During this phase, the applied load is imposed independently by both the steel and concrete components.

The lateral expansion of the concrete infill begins to rise at a particular strain and until it encounters the lateral expansion occur in steel, it continues to rise. Keep in mind that at this point, structural steel continues to expand at a consistent rate, and the concrete starts to show signs of micro cracking. The concrete's expansion is accelerated, which causes an interaction contact between the two materials. As a result, bond tensions form, putting the concrete under tri-axial stress and the structural steel under biaxial stress.[3] Some researchers, such as Knowles, have suggested that concrete confinement occurs abruptly at a strain of 0.002 when the concrete begins to dilate at 0.95 f'c. [4] On the other hand, Tsuji et al. and Zhang et al. have recommended gradually increasing concrete confinement starting at a strain of 0.001, right when

microcracking in the concrete begins, and continuing until full confinement is achieved at a strain of approximately 0.002, coinciding with the concrete's onset of swelling. [4] [5]

1.4.3 Failure modes

Due to the distinct material properties and geometric configurations of Circular Fiber-Reinforced Concrete-Filled Steel Tubes (CFSTs), it's imperative to gain insight into the potential failure modes these structural elements can undergo. Among the various modes of failure, one prevalent occurrence is the buckling of the steel tube. Interestingly, in CFST columns, this local buckling tends to manifest later than it would in an empty steel tube. This delayed onset can be predominantly attributed to the presence of concrete filling within the tube, which acts as a robust support, preventing inward buckling of the steel tube. Instead, as the axial load intensifies, the steel tube tends to buckle outward, compelled by the restraining influence of the concrete. This outward buckling phenomenon stands as a distinctive trait of CFST columns.

Researchers have observed that augmenting the outer steel tube yield stress and increasing the thickness of its wall significantly enhances the ultimate axial stress, absolute strain value at that stress, and overall ductility of CFST specimens. This enhancement primarily stems from the intensified confinement effect and a higher steel ratio within the column. During the course of loading, a notable phenomenon referred to colloquially as the "elephant foot" emerges at both ends of the specimens. This happens because the steel tubes and concrete at the extremities of the specimen only loosely connect once they reach their maximum strength. As the axial deformation advances, an additional significant incident to note is the outward buckling that transpires at the midpoint of the specimen. It's essential to emphasize that this outward buckling is a distinctive characteristic of CFST columns, underscoring their unique structural response. Conversely, the inner steel tube within the CFST may exhibit different behavior, often demonstrating localized inward buckling deformation. [6].

1.5 Reason/Justification for the Selection of the Topic

Since we know that RCC structure have brittle behavior so it is challenging to overcome this behavior of structure. CFDST would be a good choice for overcoming these issues.

Production of CFDST has demonstrated to be ductile as well as imparting for rapid production, lighter in weight and enhancement in stability. In recent years, numerous researchers have proposed the study of CFDST elements, exploring their potential as structural columns or beams. This growing interest in CFDSTs as a structural solution has spurred extensive research efforts aimed at comprehending their strength and performance characteristics.

1.6 Objectives

- To investigate the response of double-skinned, short columns filled with concrete under compressive loads.
- The effect of shear connectors on the way that loads are transferred between the steel tubes and concrete cores of CFDST columns.
- To study the incorporation of additional confinement to the outer steel tube affect the performance and behavior of CFDST columns.

1.7 Relevance to National Needs

CFDST columns have seen a noticeable increase in use within the building industry over the past year. This growing trend can be attributed to the numerous advantages these innovative structural components provide, especially when compared to traditional composite frame structures. While the adoption of CFDST columns has been a significant development in many countries over the past four decades, it remains a relatively novel concept in the context of Pakistan's building industry. The widespread adoption of CFDST technology across the globe is a testament to its effectiveness and versatility. Various nations have integrated CFDST columns into a diverse range of construction projects, including low-rise industrial structures with beams, high-rise buildings with columns, and even arch bridges. The success stories from these countries have underscored the reliability and efficiency of CFDST as a structural solution. However, Pakistan's journey with CFDST in construction is just beginning. The research we embark upon is a pivotal step in understanding the potential of CFDST within the Pakistani building industry. The primary objective of this research is to investigate and comprehensively examine the different facets, obstacles, and potential advantages related to the implementation of CFDST columns within the context of Pakistan.

1.8 Advantages

- The construction process for this type of column is rapid.

- Even when subjected to exceptionally high axial stress levels, CFDST columns exhibit exceptional energy dissipation and ductility characteristics.

- As compared to RCC column CFDST is lighter in weight.

- In seismic areas, CFDST columns are safer and more dependable since high-strength concrete is typically utilized and brittle failure can be avoided.

1.9 Areas of Application

This research highlight the use of concrete filled double skin column. This research will be used for building where brittleness is an issue and having high axial load. It resist high axial load. Moreover, this study is expecting to provide some modifications to CFDST columns

1.10 Research methodology
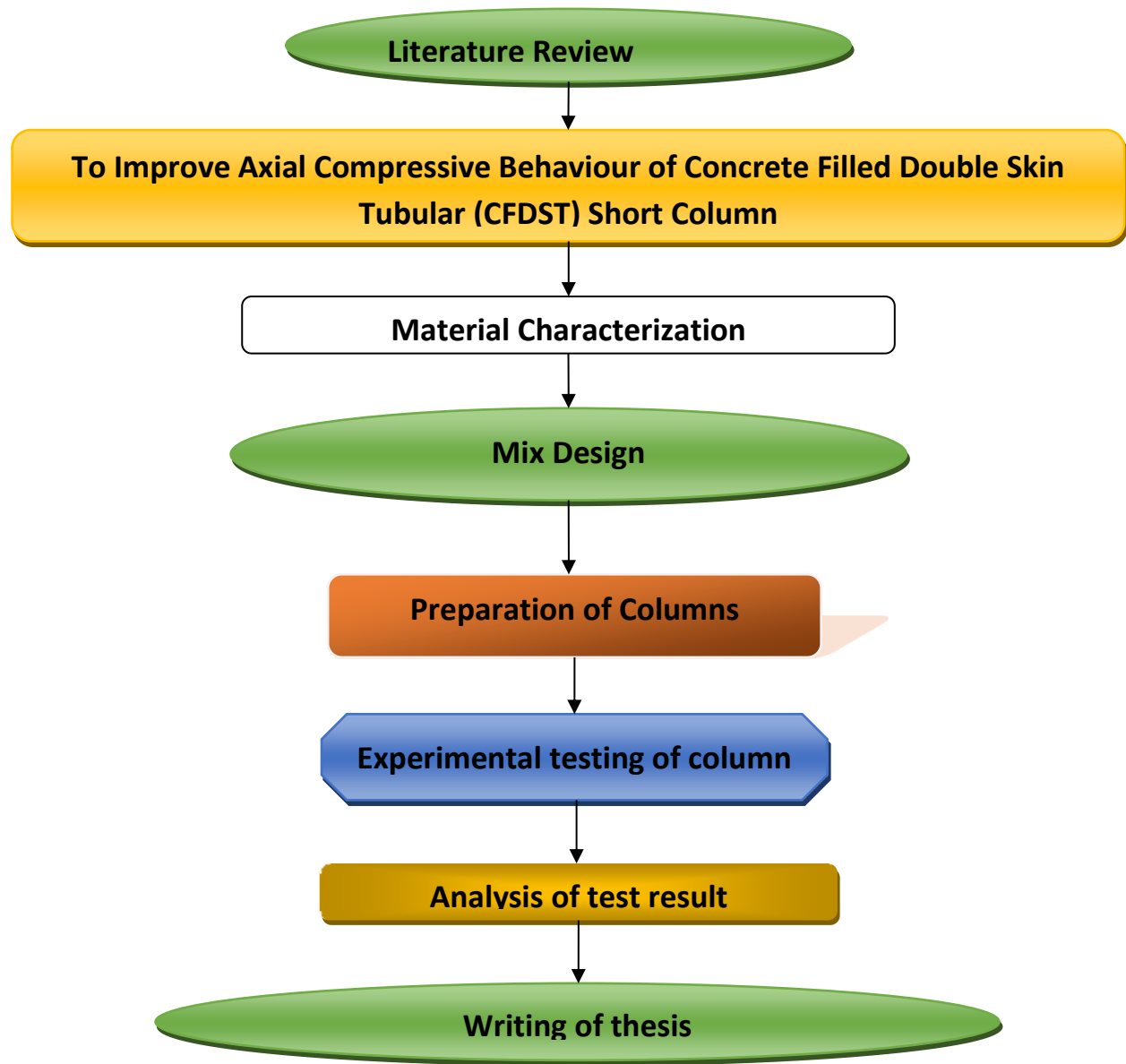
Figure 1. 2 Flow Chart of Research

1.11 Thesis layout

The research undertaken to address the aforementioned objectives is presented in five chapters.

Chapter 1 "Introduction" explains the significance of CFDST column, shape of CFDST Column, behavior of CFDST column during load, mode of the failure, research objectives, research significance, scope of the study, research methodology, and thesis outline.

In Chapter 2, titled "Literature Review," a concise overview of prior research on CFDST columns is provided.

Chapter 3 "Experimental program" discusses the test procedures and methodology. The specimen size and equipment details of this research study are presented in this chapter.

Chapter 4 "Results and Discussion" includes evaluation, analysis and discussion for results of CFDST column under the axial load. A result of LVDTs and strain gauges has also been presented.

Chapter 5 "Conclusions and Recommendations" provides the detailed conclusions based on the outcomes of this research and remarks for further studies.

LITERATURE REVIEW

Lin-Hai Han. (2006) This research focuses on examining the seismic behavior of CFDST beams and columns, utilizing recent test data as a foundation. The study encompasses various parameters, including the section types (square and circular), concrete strength, and axial load levels. To conduct this investigation, we employed 28 CFDST column samples, consisting of 12 columns with Circular Hollow Section both internally and externally, and 16 columns with Hollow Square Section for both inner and outer components. These samples underwent rigorous testing involving cyclically increasing flexural loads along with a constant axial load. The fabrication process of the CFDST samples began with the transformation of mild steel sheets into plates, which were then meticulously welded into either square or circular shapes. These shapes were subsequently joined through single-level butt welding. Interior tube surfaces were diligently cleaned through wire brushing, eliminating any rust or loose debris. Additionally, any oil or grease residues were thoroughly removed. Throughout the testing process, all composite samples displayed a ductile response, and the tests were conducted smoothly and under stringent control measures. One notable observation during the testing phase was the appearance of an outward imprint or bulge on the compression face of the composite columns. This phenomenon was consistent on both sides of the specimen. Similarly, on the opposite face of the specimen, which underwent a process involving the cutting of mild steel sheets into plates, tack welding into square or circular shapes, and final joining through single bevel butt welding, the bulge was also evident. Furthermore, the interiors of the tubes underwent thorough cleaning procedures to eliminate any presence of rust and loose contaminants, and meticulous efforts were made to remove any oil and grease buildups. Subsequently, each tube was securely welded to a square steel foundation plate with a thickness of 16 mm. One crucial finding of the research is the impact of the axial load level on the ductility of the specimens, in addition to its influence on the ultimate lateral loads. In general, as the axial load level increases, there is a reduction in the ductility of the specimens. This observation implies that the responses of the composite specimens are moderately influenced by the hollow ratio concerning lateral loads and lateral displacements. Another significant discovery was that, after reaching their peak strength, the empty tubes exhibited a rapid decrease in strength.

Son-Sub Eom. (2018) In the current study, CFDSTs—which are cheaper and lighter than CFSTs—were produced. It was suggested to splice two composite tubes together. Composite tubes with and without joints were subjected to experimental analysis as well as finite element modelling. Steel plate studs and two separate M16 shear connectors were employed. For the created CFDSTs under bending, a comparison between the ultimate loads predicted by the design calculations and the actual experimental findings was executed. Only four samples were examined with a few restrictions in this study. This paper does not take into account the effects of numerous parameters such as connector spacing, splice connection length, connection plate thickness, etc. Four distinct specimens were created for this experiment. Two examples were created for every shear connection variation (M16 and plate studs), one with and one without the joint. Concrete filled the spaces between the tubes and between the sample's inner and outer steel tubes. These steel tubes had the shear connectors welded onto them. In this work, double-skinned steel tubes with or without a junction filled with concrete were constructed. Through the experiment and analysis, Four different composite tubes' flexural behaviour and performance were studied. The results led to the following conclusions. Because the experiment's findings and the FEA's findings match, It was confirmed that the composite tubes' produced FE model was accurate. The model is applicable to composite tubes of various sizes. Under the maximum force, the steel plate studs broke, but not the M16 studs. M16 studs work better than steel plate studs in this situation. The results from finite element analysis (FEA) indicated that the joint possesses adequate strength to connect these composite tubes, and testing for the composite tubes with the junction. The investigation's findings support the idea that the created CFDST components have enough flexural strength to be used in building.

Lin-Hai Han (2010) Fiber-reinforced polymer (FRP) composites have grown significantly in popularity among the civil engineering community in recent years. The numerous benefits that FRP composites have over more traditional structural materials like steel and concrete are largely to blame for this increased attention. High strength and superior corrosion resistance are two of these benefits. As a result, there is rising interest in using FRP composites into a range of civil engineering projects, including both new construction initiatives and the retrofitting of existing structures. As a result, a lot of research has been done to examine the behavior and effectiveness of structures built utilizing FRP composites in combination with other materials. The composite members' performance under cyclic loading is still not well understood. It suggests that more study

in this area is necessary. 8 FRP concrete and steel DSTCs were examined in this study under conditions of cyclically increasing flexural force and constant axial load. The amount of FRP layers and the axial load level are the two primary determinants in the experiment. It was investigated how different properties affected stiffness, ductility, strength, and energy dissipation. Up until the specimen's strength declined to around 50% of its peak load. The tests were carried out while being loaded cyclically, at which point the normal lateral loading pattern began. 3.75 mm was the specimen's mid-span displacement, and the rotation increment was calculated to be 0.005 rad. As a result, the mid-span displacement of the three cycles were included in the cyclic loading history, which was 3.75, 7.5, and 11.25 mm. After attaining the failure load, the DSTC specimen made of FRP concrete and steel remained unchanged, at the reaction blocks till it buckled. All tested specimens have failure modes that are often rather similar. The sample were set to air-dry when one of them experienced a longitudinal FRP jacket break, according to observations made throughout the entire failure process. At the top of the column, relatively little longitudinal shrinkage happened during curing. Using the inner steel tube, the surface of concrete must be level, this longitudinal gap was filled with a high-strength epoxy. Finally, FRP wrapped the samples using a hand lay-up technique. It is concluded that before the longitudinal FRP ruptures, DSTC specimens of FRP-concrete and steel structures frequently exhibit substantial levels of energy dissipation, followed by a sharp decline in lateral load capability Given that the current tests' scope includes an axial compressive load, The FRP-concrete-steel DSTC's seismic performance can be improved to some extent. It should be highlighted that in some cases, better ductility capabilities for the composite columns may be required to mitigate the effects of an unanticipated FRP rupture, according to the experimental investigation presented in the paper. As a result due to the use of a larger steel tube for this reason, the FRP's contribution to the overall strength will diminish. However, as the inner steel tube's dimensions grow, Its higher sectional slenderness ratio will probably cause severe local buckling in response to the reverse lateral loading. A suitable parameter must be found for each FRP and concrete-steel DSTC component., more work needs be done to build a numerical model and explore the parameters.

Xi-Feng Yan (2021) This research was dedicated to investigating the structural behavior of short columns subjected to axial loading, possessing a concrete core and a circular cross-sectional shape. The study adopted a comprehensive approach by combining experimental and numerical methods to assess the performance of Concrete-Filled Double Skin Tubular (CFDST) columns, which

featured both inner and outer steel tubes. A total of 28 test runs were conducted to thoroughly examine how these columns behaved under various conditions. The study employed six different sectional dimensions for the circular hollow steel tubes, which served as both inner and outer skins in the experiments. The outer skins were fabricated from STK490 steel tubes with dimensions of 190.7x5.3 mm, 190.7x6.8 mm, and 190.7x5.3 mm, while the inner skins were crafted from STK400 steel tubes measuring 190.7x4.3 mm. Each inner skin had dimensions of 60.5 mm by 3.8 mm. To ensure consistent material properties, tensile coupons were extracted from the same parent material as the test specimens, utilizing the curved face of the circular hollow steel (CHS) tubes as a template. The study also characterized the concrete used through standard concrete cylinder tests. Three distinct concrete grades—C24, C36, and C48—underwent testing on six typical concrete cylinder specimens each, following a 28-day curing period. The test results indicated compressive strengths of 48.2 MPa, 34.2 MPa, and 21.7 MPa for C24, C36, and C48, respectively, with variance coefficients of 0.024, 0.008, and 0.031. All testing procedures were conducted utilizing a universal testing machine with a 5000 kN compression capacity. The study's conclusions highlighted that the yield stress and hollow ratio of the outer steel tube had a negligible impact on the initial stiffness of the columns. Conversely, factors such as the thickness of the outer tube's skin played a pivotal role. Specifically, an increase in concrete strength from 24 MPa to 48 MPa resulted in a 12.8% rise in initial stiffness. Furthermore, when the wall thickness of the outer tube skin was augmented from 4.3 mm to 6.8 mm, the initial stiffness of the columns increased significantly by 39.2%. Columns with varying thicknesses of the outer steel tube skin exhibited distinct failure modes and patterns, highlighting the substantial influence of yield stress and wall thickness on the failure mechanisms of these steel tube columns.

Hussein Ghanim Hasan (2021) Check out the Bond-slip behavior of CFDST columns. This paper delivers new results and significant insights for the bond-slip industry because there is a dearth of information on the behavior of CFDST columns when they slip. No studies have focused on how welded reinforcing bars affect the bonding behavior of composite columns. Modest D/t ratios were determined and chosen for the internal and external steel tubes to ensure appropriate bond strength and prevent any local tube buckling under stress.16 CFDST specimens with internal tube diameters of 76.1 mm and external tube diameters of 168.3 mm were constructed and evaluated. For all examples, the steel-concrete interface was intended to be 300 mm long. The tensile strength averages for the HSC and NSC were 6.4 MPa and 4.5 MPa, respectively, according to the test

results. Twelve CFDST stub columns had internal rings, the first four sample were manufactured having no additional interface types, whereas the final four were made with reinforcing bars, or shear studs, put into the inner tubes to boost the bond strength. A testing device with a 3000 kN capacity was used to test all specimens. For each column, a single L/D value was chosen. The slide at the testing end was also calculated using LVDTs. The bond failure modes are examined in terms of the failure type, taking into account the tubes, internal rings, shear studs, shell concrete failure modes and reinforcing bars. Typically, adhesion, friction, and sliding are considered to be the three main mechanisms responsible for the shear strength shown in push-out tests. The outcomes show that the internal rings and reinforcing bars welded to the inner tube can significantly increase the CFDST specimens' interface components' interfacial binding strength. While providing less shear resistance than other interface types, shear studs (bolts) inserted into inner steel tubes can strengthen the binding. The main cause of this is the surface imperfections, which allow the shell concrete and the inner steel tube to mechanically interlock. As the strength of the concrete shell improves, so does the bonding strength. This is because of the adhesive force's significant enhancement of the bond strength's shear resistance. The pullout mode of failure for welded reinforcing bars in specimens filled with low strength concrete was crushing and shearing of the area around the bars, but it was not present for welded reinforcing bars in specimens filled with high strength concrete.

Hui Zhao (2020) The primary aim of this study was to investigate the behavior of slender columns and beams within CFDST structures that feature an external stainless steel tube. The research employed a combination of experimental analysis and computational modeling to comprehensively understand the performance of these structural elements. The study involved a total of eighteen specimens, including twelve slender columns and six beams. The choice of stainless steel as the material for the external tube was driven by its exceptional resistance to corrosion, high impact resistance, fire resistance, and ease of maintenance. Stainless steel has gained increasing popularity in recent years for structural applications due to these advantageous properties. Notably, stainless steel exhibits a high strain-hardening capacity without a distinct yield strength, resulting in exceptional ductility, with the ability to elongate by nearly 50% after fracturing. An hydraulic compression machine with a 5000 KN capacity was used to test column specimens experimentally. Knife edges at both ends of the specimens and high-strength 6 mm deep groove steel plates allowed for the creation of pinned boundary conditions and a range of loading

eccentricities. Finite Element (FE) models were created to further examine the behavior of CFDST structures and reproduce the experimental results. In parametric research, these models were utilized to investigate important characteristics such the hollow ratio, load eccentricity, and material strength. The investigation of load distribution among various components and contact strain between the steel tubes and the sandwiched concrete was made easier by the FE models. The study's findings showed that the thin columns and beams exhibited ductile behavior, with the double-skin tubes playing a vital role in containing and maintaining the integrity of the sandwiched concrete. Similar to those seen in carbon steel, which is employed in both CFST and CFDST members, failure patterns were seen in CFDST members with outside stainless steel tubes. According to the experimental data, the FE models accurately predicted load-bearing capacity and load-deflection behavior.

Xi-Feng Yan (2021) A comprehensive experimental program was undertaken, involving a total of 24 specimens constructed from both HSC and UHSC, with the aim of investigating the compressive behavior of short CFDST columns. The primary objective of this study was to evaluate the compressive strength characteristics of these circular CFDST columns when filled with different concrete strengths. Three distinct types of concrete were utilized, each possessing varying cylinder compressive strengths of 83 MPa, 46 MPa, and 130 MPa, to fill the column specimens. Particular attention was paid to the precise preparation of the specimens using concrete mortar to ensure uniformity and compatibility with the steel tube. This was particularly crucial because the upper portion of the concrete had a tendency to shrink during curing, necessitating precise alignment with the steel tube. After the concrete had fully cured, the bottom endplate was removed to prepare the specimens for testing. All specimens were subjected to loading on a universal testing machine UTM with a maximum compression capacity of 5000 KN. Axial load and displacement data were collected using pressure sensors integrated into the UTM and Linear Variable Differential Transformers LVDTs, respectively. The test results yielded valuable insights into the compressive behavior of round CFDST columns under varying concrete strengths. The findings indicated that the use of stronger concrete typically resulted in higher axial strengths and initial stiffness. It was observed that as the concrete strength increased, the absolute strain value at the point of ultimate axial stress decreased, primarily due to the inherent brittleness of HSC and UHSC materials. Both the ultimate axial stress and the absolute strain value at that stress were significantly influenced by the hollow ratio of the exterior steel tubes. A higher hollow ratio led to

lower ultimate axial stress and reduced absolute strain. Conversely, increasing the yield stress and wall thickness of the outer steel tube had a positive effect on ductility, absolute strain at ultimate axial stress, and ultimate axial stress. This improvement was attributed to the increased steel ratio and enhanced confinement effect in the columns. The behavior of the CFDST columns was characterized by the inward bending of the inner tubes and outward buckling of the outer tubes, typically occurring around mid-height. It was determined that several factors, including concrete compressive strength, influenced this behavior. Increases in concrete strength, wall thickness, and outer tube yield stress were found to result in increased cross-sectional resistance for the CFDST columns, which exhibited a linear correlation with concrete strength.

Muhammad Usman (2019) The principal aim of this research is to investigate the confined axial compressive behavior of High Strength Steel Fiber Concrete (SFRC) and explore strategies to mitigate the inherent brittleness of High Strength Concrete (HSC) through composite action. The focus on this research area has grown significantly due to the superior strength, durability, and performance attributes associated with HSC. The study delves into how the incorporation of steel fibers into HSC, in conjunction with ductile materials, can alleviate the intrinsic brittleness of concrete and augment its performance. To execute this experimental investigation, a total of 39 high-strength concrete (HSC) cylinders were cast. These cylinders featured various steel fiber volume fractions (Vf), specifically set at 0.5%, 1.5%, and 2.5%. Among these samples, nine were cast directly within steel tubes, while 18 were enclosed with Fiber Reinforced Polymer (FRP) sheets after a 28-day curing period. Following this curing period, a particular sample identified as UC-UR demonstrated a compressive strength of 50.67 MPa. The stress-strain curves derived from the experiment reveal that the peak stress was attained at an average strain value (eco) of 0.235%. These specimens exhibited a brittle failure mode, characterized by an abrupt drop in the stress curve. Interestingly, the addition of steel fibers had a limited impact on enhancing compressive strength. However, it led to a noticeable increase in strain values, spanning from 10% to 15%. Furthermore, a higher steel fiber content corresponded to an increase in peak strain. What is particularly intriguing is that the reduction in concrete strength after reaching the peak load was not as sudden as observed in the control samples. Additionally, there was a notable reduction in the typical, sudden failure characteristic of concrete. Even after reaching the peak strain, the presence of steel fibers prevented immediate failure by bridging the cracks and allowing for further strain.

Kojiro Uenaka (2015) This research primarily focused on investigating the compressive behavior of CS-CFDST (Concrete-Filled Double Skin Tubular) short columns, which have a unique structural configuration with inner square and outer circular sections. These columns consist of an inner square hollow steel section and an outer circular hollow steel section with concrete filling in between. This design offers various advantages, including reduced weight compared to columns with conventional fills, making them suitable for seismic-resistant constructions. The study aimed to explore the behavior of CS-CFDST columns by adjusting two critical testing parameters. The outer circular steel tube's diameter-to-thickness ratio, which varied in the range of 69 to 160. The ratio of the inner width to the outer diameter, which ranged from 0.0 to 0.5. By systematically varying these parameters, the research covered a wide range of combinations to assess their impact on the performance of CS-CFDST columns. One significant observation from the study was that the presence of the surrounding poured concrete led to deformation of the inner square steel tubes, resulting in a hollow shape. In cases where the inner width was 80 mm, the axial deformability of the CS-CFDST columns was found to be less than 0.33. This value was lower than the inner width-to-diameter ratio, indicating limited axial deformability of the columns under these conditions. However, it was noteworthy that the axial loading capacity of the CS-CFDST columns either matched or exceeded the expected values, particularly when considering the combined strength of the inner and outer steel tubes along with the filled concrete. These findings underscored the durability and load-carrying capability of CS-CFDST columns, even when they exhibited minor axial deformability.

Tao Zhang (2020) This research is focused on investigating the compressive behavior of short columns made from circular steel tubes filled with reinforced concrete, commonly known as SRCFT stub columns. SRCFT stub columns are a promising type of composite column with potential applications in various engineering structures, including piers and columns. To accurately anticipate SRCFT stub columns' compressive strength and ensure their efficient application in engineering design, it is essential to comprehend their compressive behavior. The study employs a combination of numerical simulations and experimental testing, involving a total of eight test samples. These samples consist of four CFT stub columns and four SRCFT stub columns. The study explores how variables like steel section design and concrete strength can impact how well SRCFT stub columns function. The exterior surface of the tubes is painted red, and 50 mm white grids are painstakingly marked on the painted surface to allow for the monitoring of deformation

and failure. In order to ensure exact alignment at the tube's center, a cover plate is carefully welded to one end of the circular steel tube to prepare the specimens. Concrete is then poured into the specimens from the top, with the use of a vibrator to ensure even distribution within the tube. The top surface of the concrete is meticulously smoothed to align with the level of the steel tube. For conducting compressive tests, hydraulic testing equipment with a capacity of 2000 T is utilized. LVDT are strategically positioned at the mid-height of the tube's exterior surface, and four strain rosettes are affixed to the tube to provide precise measurements of deformation. One noteworthy discovery in this research is the pivotal role played by the steel insert in SRCFT stub columns in influencing their failure modes. It effectively retards or even prevents the propagation of shear cracks within the concrete core, leading to an enhancement in ductility. Ductility, in this context, refers to the capacity of the columns to deform significantly before reaching failure. In comparison to conventional CFT short columns, SRCFT stub columns tend to exhibit superior ductility, which is a highly desirable characteristic in structural engineering. This study also underscores that both the design of the steel section and the strength of the concrete exert significant influence on the ductility, ultimate bearing capacity, and strength-to-weight ratio of SRCFT stub columns. While higher ultimate bearing capacity tends to reduce ductility, the design of the steel section enhances both ductility and ultimate bearing capacity, contributing to a greater reserve of energy within the columns. This heightened performance renders SRCFT stub columns more reliable under various loading conditions.

Stelios Vernardos (2019) This study offers a comprehensive examination of the experimental performance of stubs constructed from CFDST components. Over several decades, extensive research has firmly established CFDST members as a structural concept that is on par with traditional steel tubular members and CFST members. It also serves as a potent illustration of how steel and concrete may work together effectively in structural systems. This innovative concept emerged as a potentially effective solution to address the challenges associated with CFST members, which were originally designed to enhance the performance of conventional steel tubular members. The research undertaking involved a comprehensive analysis of multiple experimental projects conducted over a span of 20 years, with a primary focus on the compressive behavior of short CFDST components. The results of these experiments have been summarized to unveil critical insights into the structural response and common failure mechanisms observed across various cross-section forms and geometrical parameters. Through an extensive analysis of

experimental investigations, several key characteristics have come to light. The majority of CFDST specimens have demonstrated notably high axial capacity, underscoring their structural robustness and load-bearing capability. Furthermore, these specimens have exhibited a high degree of ductility, signifying their capacity to undergo significant deformation before reaching failure. This ductile behavior holds significant value in structural components, as it enables energy dissipation during extreme loading conditions. The research has highlighted the effectiveness of the CFDST concept in terms of energy absorption and strength. This was quantified by calculating the ratio of the maximum load attained by each CFDST specimen to the sum of the maximum loads of its individual components. Additionally, the study determined the maximum amount of energy that each CFDST specimen could absorb. The findings derived from this study provide substantial evidence for the efficacy of the CFDST concept in the realm of structural engineering. CFDST members not only demonstrate impressive axial capacity and ductility but also excel in terms of energy absorption. These attributes position CFDST as an appealing choice for a wide range of engineering projects where structural integrity and resilience are of paramount importance.

<div align="right">**CHAPTER 3**</div>

EXPERIMNTAL PROGRAM

3.1   General

In this chapter, we will thoroughly outline the methodology employed to accomplish the research objectives. We will offer comprehensive explanations of the procedures involved in preparing the specimens and the testing techniques utilized to obtain our results. Our study focuses on analyzing the compressive strength of CFDST columns under various outer steel tube geometric conditions. We cast a total of 8 specimens to accomplish this. Previous research on CFDST columns has shown that failure often results from the outer steel tube yielding, which causes outward buckling at the specimens' mid-height as axial distortion advances. Our main goal is to improve the axial compressive performance of CFDST columns while keeping the steel tube's overall thickness constant. Instead of uniformly increasing the thickness, we have adopted a novel approach. To solve the issue of the weak mutual constraint between the concrete and steel tube at both ends of the specimens under loading, we have inserted shear connectors on the inner side of the outer steel tube and the outer side of the inner tube at various intervals. Concrete is then placed between these shear connectors. To explore the compressive strength of CFDST columns while taking diverse geometric parameters of the outer steel tube into account, a total of 8 specimens have been cast. Our research primarily focuses on improving the behavior of the outer steel tube, a critical component in CFDST columns. Rather than increasing the overall thickness of the steel tube uniformly, we have chosen to strengthen the critical zone of the specimen. The incorporation of shear connectors and the reinforcement of this critical zone are anticipated to enhance the behavior of CFDST columns. By addressing issues related to the behavior of the outer steel tube, our research aims to provide valuable insights to the field of structural engineering. In the upcoming sections, we will provide a step-by-step account of the specimen preparation process, which includes casting the specimens and implementing the shear connectors.

3.2   Material

High-strength concrete, steel tubes, and shear connectors were used to construct the CFDST short columns used in this study. Each column comprises two steel tubes: an inner

tube with a smaller diameter and an outer tube. The inner tube is precisely centered within the outer tube, and high-strength concrete is placed between these concentric tubes. We have used M16 studs as shear connectors to ensure efficient shear transfer between the steel tubes and the concrete core. These connectors play a pivotal role in enhancing the structural integrity and performance of the CFDST columns.

3.2.1 High Strength Concrete

The compressive strength of concrete is an important factor in determining the overall strength and durability of a structure made of reinforced concrete. The strength of the concrete in a structure is typically determined by testing cylindrical or cubic specimens that are molded and cured under standard laboratory conditions. Concrete, which is sandwiched between the inner and outer steel tube, are high strength concrete. The concrete mix design comprises of one portion of cement, 1.52 portion of fine aggregate and 2.41 portion of coarse aggregate. The water cement ratio used for this concrete is 0.52. Concrete admixture whose addition improve concrete quality in both wet and hardened state were used in this mix design. Silica Fume was employed as an admixture in this investigation. Silica fume has a high density and a tiny average particle size, resulting in a better microstructure in the concrete. The silica fume utilized had a bulk density of 660 kg/m3. Sika Chemical (PVT) LTD, a chemical supplier that also manufactures silica fume, obtained it. To prepare a workable concrete mix at a very low water-cement ratio, superplasticizer was used. The commercial name of superplasticizer is chemrite 303 SP. 0.5% of super plasticizer 4% of condensed silica fume and 2% of steel fiber were used in mix design.

Table 3. 1 Concrete mix Design

Mix proportions (to the weight of cement)						
Cement	Water	Fine Aggregate	Coarse Aggregate	SP	CSF	Fibers
1	0.52	1.52	2.41	0.005	0.04	0.02

To rectify the control mix design, we implemented the concrete mix design listed in Table.3.1. Subsequently, the casted cylinders were immersed in a curing tank for a duration

of 28 days. Following this curing period, we conducted compression tests on six standard concrete cylinder specimens using a compression testing machine.

Figure 3. 1 Concrete cylinder for compressive test in UTM

3.2.2   Steel Tubes

A CFDST column is a structural column configuration consisting of two steel tubes arranged concentrically. The outer steel tube typically adopts a circular or rectangular shape, while the inner steel tube retains its circular form. Concrete is then placed in the space between these outer and inner tubes, forming the core load-bearing element of the column. In the CFDST columns used for this research, two steel tubes of different diameters were employed. The larger diameter steel tube was designated for the outer layer, while the smaller diameter tube was utilized for the inner layer. Specifically, in our study, we employed circular tubes with distinct diameters. The outer steel tube maintained a constant diameter of 152.4 mm in all specimens, while the inner steel tube had a consistent diameter of 50.8 mm across

all cases. Additionally, the wall thickness of these CFDST columns was modified to either 1 mm or 2 mm for the outer steel layer.

The wall thickness of the inner steel tube for the entire specimen was fixed which is 1mm.

Table 3. 2Material properties of internal and external tubes

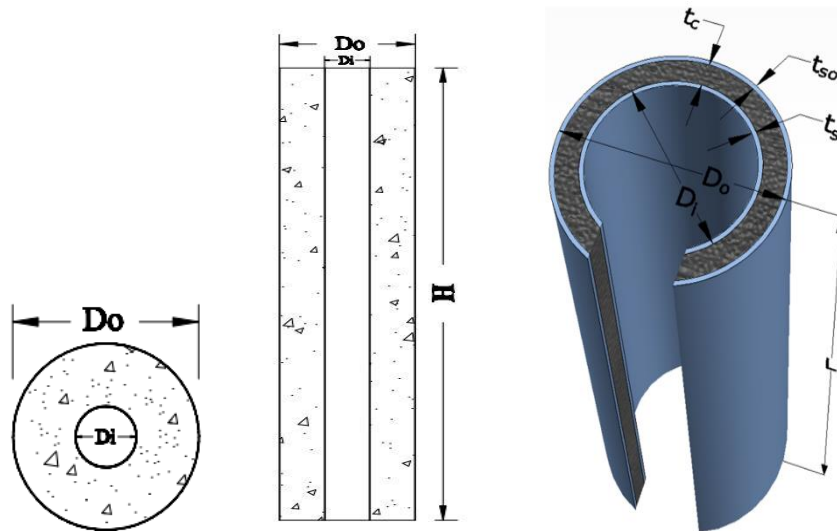| Series	Location	Section size (mm)	fsy (Mpa)	fsu (Mpa)	$E_{\circ}$ (Gpa)
1	External tube	152.4 x 1	410	460	200
	Internal tube	50.8 x 1	410	460	200
2	External tube	152.4 x 2	410	460	200
	Internal tube	50.8 x 1	410	460	200

Figure 3. 2 Detail of CFDST Column

Where as

- Do represents the external diameter of the outer steel tube.
- Di represents the external diameter of the inner steel tube.
- Tc represents the thickness of the concrete core.
- Tsi represents the thickness of the inner steel tube.
- Tso represents the thickness of the outer steel tube.

23

Getting coupon samples from each of the two steel tubes that were bought has two main goals. Firstly, it is essential for acquiring critical steel properties such as yield strength and fracture strength, which are fundamental for subsequent analysis and calculations. Secondly, it serves to confirm that the two steel tubes possess comparable properties. In cases where there are significant differences in properties, it necessitates the consideration of new parameters when comparing the specimens.

The coupon specimens dimensions needed for testing can vary depending on various factors, including the available testing equipment. Figure 3.3 illustrates one of the measurements for a steel coupon sample. These specimens are created using remnants from the steel tubes.
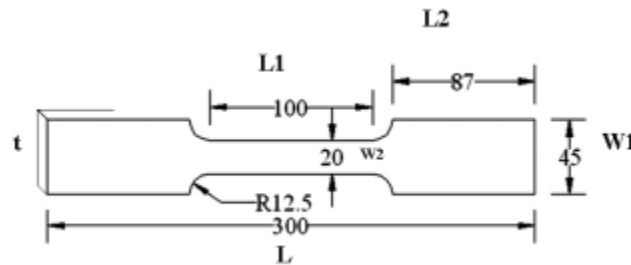
Figure 3. 3 Coupon Test Sample Dimensions

3.3 Shear Connector

In Concrete filled double skin column or beam the slip, occur between concrete and steel during loading. To overcome this issue we provide shear studs M6 having 16mm in length. The design procedure for the shear connector is developed in accordance with LRFD principles, and it is summarized as follows:

First step is to choose the type of shear connector which are using its dimension and material properties

- Calculate the nominal shear force of the considered area using the provided formula.

$$P = [As.Fy; 0.85f'_c.Ac]$$

- Calculate the shear resistance of a shear connector :

24

$$Q_n = 0.5A_{sc}\sqrt{f'_c E_c} \leq A_{sc}F_u$$

- Calculate the number of Studs

$$n = \frac{P}{\phi_{sc}Q_n}$$

- Calculate the spacing of stud

$$d_{stud} = \frac{L_{tube}}{2n}$$

where,

The design parameters and equations for the shear connector are crucial components in our analysis:

As and Fy: These denote the cross-sectional area and yield strength of the outer tubes, respectively.

fc' and Ac: Stand for the concrete's compressive strength and area in the given section, respectively.

Asc and Fu: These are, respectively, a stud shear connector's cross-sectional area and minimum tensile strength.

φsc: stands for the shear connections' resistance factor.

Ltube: Signifies the length of the composite tubes.

To determine the number and spacing of studs for a given section, we employed two types of specimens in our study: C-WSC (Column without shear connector) and C-SC (Column with shear connector). This approach allowed us to extrapolate the findings from one part of the composite tube to other sections, ensuring a comprehensive analysis of the entire structure.

Table 3. 3 Shear Connector Detail

	Specimens	Shear Connector	Di X Tsi (mm)	Do X Tso (mm)
Series-1				
	C-WSC	No	50.8x1	152.4 x 1
Series-2				
	C-SC	Yes	50.8x1	152.4 x 1

3.4 Test Specimen

In this study, we produced a total of eight specimens of CFDST short columns for experimentation. These specimens were divided into three main groups, each with distinct characteristics related to the inclusion of shear connectors, reinforcement of the outer steel tube, and variations in the thickness of the outer steel tube.

3.4.1 Strengthening of outer steel tube

In a previous study, it was demonstrated that concrete-filled double steel columns often experienced failure due to a combination of local failure within the column and yielding of the steel tube. Notably, a noticeable outward indentation or bulging occurred around the stub as the steel approached its yield strain. This effect was clearly visible on both sides of the stub at the compression face of the composite column. This observation emphasized the importance of two key factors: the thickness of the outer steel tube wall and the yield strength of the outer steel tube, both of which had a significant impact on the failure mode of CFDST columns. To address this challenge, rather than uniformly increasing the overall thickness of the outer steel tube, we chose to implement additional reinforcement measures specifically targeted at the critical zone of the outer tube. These measures are detailed in Table 03 and are aimed at enhancing the structural integrity and performance of the CFDST columns.

In C1-1mm the overall thickness of the inner and outer steel tube were 1mm. This type of sample would be considered as control mix. C1-1Do having extra stirrup of width Do/2 at top, bottom, and Do at the center of the Column. At C1-1.5Do having extra stirrup of width Do/2 at top, bottom, and 1.5Do at the center of the Column. At C1-2Do having extra stirrup of width Do/2 at top, bottom, and 2Do at the center

of the Column. At C1-Do/2 having extra stirrup of width Do/2 throughout the span of the column. C2-2mm having double outer wall thickness to C1-1mm. The last two sample of both series will be compare with the above sample. This comparison would tell us about the strengthening of the critical zone only to increasing the whole thickness of the tube.

Table 3. 4 Strengthening of Outer Steel Tube

Series	Specimens	Top	Middle	Bottom	Di X Ti (mm)	Do X To (mm)
Series-1	C1-1mm	-----	----	----	50.8x1	152.4 x 1
Series-2	C1-Do/2	$D_o/2$	$D_o/2$	$D_o/2$	50.8x1	152.4 x 1
	C1-Do	$D_o/2$	D_o	$D_o/2$	50.8x1	152.4 x 1
	C1-1.5Do	$D_o/2$	$1.5\,D_o$	$D_o/2$	50.8x1	152.4 x 1
	C1-2Do	$D_o/2$	$2\,D_o$	$D_o/2$	50.8x1	152.4 x 1
Series-3	C2-2mm	----	----	----	50.8x1	152.4 x 2

Figure 3. 4 (a) CFDST Short Column

Figure 3. 5 Detail of Outer Steel Tubes
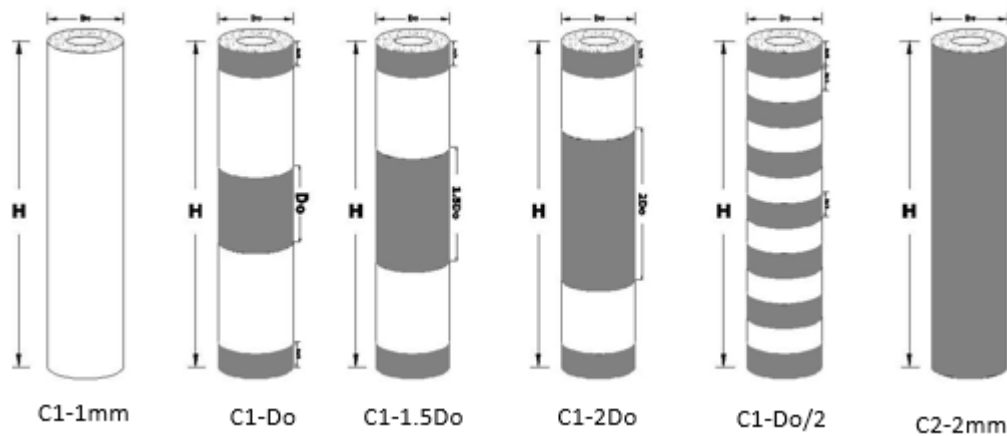
3.5   CFDST short Column Casting

The mix proportion discussed above used for the concrete mix design. Silica Fume was employed as an admixture in this investigation. Silica fume has a high density and a tiny average particle size, resulting in a better microstructure in the concrete. The silica fume utilized had a bulk density of 660 kg/m3. Sika Chemical (PVT) LTD, a chemical supplier

that also manufactures silica fume, obtained it. To prepare a workable concrete mix at a very low water-cement ratio, superplasticizer was used. The commercial name of superplasticizer is chemrite 303 SP. 0.5% of super plasticizer 4% of condensed silica fume and 2% of steel fiber were used in mix design. The mixing of the concrete ingredients was done with a horizontal concrete mixer as shown in figure. The mixing of different concrete elements was done according to the specifications provided by (ASTM C192 / C192M 2016) (Standard 2016). The following is a summary of the mixing technique. The mixing water was separated into four parts at first, and then superplasticizer was added to one of the quarters.

To begin, coarse aggregates were added to the mixer, along with about a quarter cup of mixing water, and the mixture was allowed to mix for about 2-3 minutes. Second, after adding fine aggregates, the mixture was mixed for another 2 minutes. Third, the binder (cement plus silica fume) was added, along with about two-thirds of the mixing water, and thoroughly mixed.

Figure 3. 6 Concrete Mixer

Finally, the leftover superplasticizer was mixed with a quarter of water and the entire mixture was allowed to mix until it reached a homogeneous consistency. The concrete mixer machine was then turned off and allowed to rest for three to four minutes. After the

rest, the mixing was continued, with a final mixing time of 2 minutes. At time of casting 3 cylinder were casted in every batch to check the compressive strength of concrete at every batch. The concrete is poured between the two tubes and the specimen is placed on the vibrator for the proper compaction of concrete mix. Total 16 Specimen were casted in concrete Lab of MCE.

3.6   Curing of CFDST Column

The curing process for CFDST columns in the lab is similar to that of other concrete structures. After the concrete is placed in the steel tube, it is important to keep the concrete moist and at an appropriate temperature to allow it to harden and gain strength. This can be achieved by covering the column with wet burlap or plastic sheeting and keeping it in a temperature-controlled environment, such as a curing room or chamber.

The duration of the curing process for CFDST columns will depend on a number of factors, including the type of concrete used, the ambient temperature, and the humidity levels. In general, however, CFDST columns were placed at MCE concrete lab curing tank for 28 days to allow the concrete to reach its full strength and durability. During the curing process, it is important to monitor the column for any signs of cracking or other defects, and to take steps to address any issues as they arise. After 28 days remove all the samples from the curing tank and is ready for testing.

Figure 3. 7 Casted CFDST Short Column

3.7 Testing Setup for CFDST Short Column

The test procedure entails the application of a compressive force to a concrete-filled double-skin column until it reaches failure, with continuous monitoring of load and deformation throughout the test. In a typical compressive test for a concrete-filled double-skin column, the column is positioned between two loading platens, and hydraulic jacks or similar equipment are used to incrementally apply compressive loads. Throughout the test, the deformation of the column is closely tracked, and the load at which failure occurs is documented. The outcomes of the compressive test serve multiple purposes, including the calculation of the compressive strength of both the concrete and steel components, as well as an examination of the column's behavior under different loading scenarios. It is essential to adhere to established testing standards, such as ASTM C39 for concrete-filled cylindrical columns, to ensure the accuracy and consistency of the results.

Using a universal testing machine installed in the MTL Lab at the University of Engineering and Technology Peshawar, all CFDST specimens were put under a continuous axial load.

The test specimens were 660mm in length. All of the specimens were tested using a universal testing machine (UTM) with a compression capacity of 2000 kN. The above figure demonstrates how top and bottom ring bearing plates were used to apply axial compressive forces to both ends of each specimen.

3.7.1 Universal Testing Machine

The universal testing machine employed for the compression tests on all specimens, except for the coupon steel samples, was the MTS Servo Hydraulic Compression Model YAW4306. The sizes and capacities of the samples were meticulously determined to ensure they did not surpass the limitations of the testing machine, specifically with regard to specimen height and compression capacity. It's worth noting that the load-deformation graphs presented in subsequent chapters were generated using data collected from the built-in gauges of the machines. The measurements of the specimens were prepared in accordance with the relevant standards, taking into account the capacities of the machines.

Figure 3. 8 Testing of CFDST Short Column in UTM

The ends of the specimens were slightly larger in size compared to the gripping heads of the testing machine. It's important to note that despite this size difference, there was no

slippage of the samples during any of the conducted tests. For a visual representation of the experimental setup, please refer to the figure illustrating the configuration of the two universal testing machines.

3.7.2 Strain Gauges

During the testing process, unidirectional strain gages were employed for measurements. These strain gages were specifically utilized to measure the strains experienced by steel surfaces, including those of the CFDST steel tube. Detailed characteristics and specifications of these strain gages are provided in the accompanying Table.
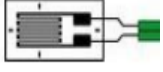
Strain Gauge Pattern	Nominal Resistance (Ω)	Approximate Gauge Factor	Dimension (mm)	
			Grid	
	120	2.01	Length	Width
			5	3

Figure 3. 9 CFDST Column with Strain Gauges

To ensure precise measurements, it was imperative to shield the exposed sections of the strain gage's wire from direct contact with the conductive surface of the steel. This safeguard was achieved by applying masking tape both below and above the exposed part of the wire.

For consistency, the strain gages were uniformly affixed in the mid-height region of the specimens, with each specimen being equipped with one gages oriented horizontally. To provide a visual reference, Figure3.9 depicts photographs of the strain gauges utilized in the conducted experimental tests.

<div align="right">**CHAPTER 4**</div>

RESULTS AND DISCUSSIONS

4.1　Introduction

This chapter summarizes and analyses the results of tests done on CFDST specimens, including compressive strength of CFDST short column, effect of share connector, failure mode, comparison of strain values at different location of the column and effect of stabilizing the critical zone with respect to increasing the overall thickness. Along with checking the mechanical qualities, visual observations were taken to determine how the failure mode of all samples changed after providing the extra strength at the critical zone of the column.

4.2　Concrete Material Test

Concrete cylinders were cast from the same concrete batches used to fill the CFDST short columns. For each batch, three cylinders were produced. Following a curing period of 28 days in water, nine standard-sized concrete cylinders were selected to undergo a standard compressive test. This test aimed to determine the compressive strengths of the three concrete batches. The testing procedure for concrete cylinders typically adheres to standards such as ASTM C39/C39M, which is widely accepted for assessing the compressive strength of concrete cylinders. According to ASTM C39/C39M guidelines, the loading rate for testing concrete cylinders should fall within the range of 0.14 to 0.34 MPa per second (equivalent to 20 to 50 psi per second). The selection of this loading rate is of paramount importance, as it can significantly impact the test results and influence the measured compressive strength of the concrete.

Figure 4. 1 Concrete Cylinder Under UTM

If the loading rate is too fast, the test may produce artificially high strength values, as the concrete may not have enough time to deform and redistribute stresses before it fails. On the other hand, if the loading rate is too slow, the test may produce artificially low strength values, as the concrete may creep and develop micro cracks over time.

Table 4. 1 Test Result of Concrete Cylinder

S.No	Description	Cylinder Strength(Mpa)	Avg. Compressive Strength (Mpa)
Batch-1	C-1-a	43.7	43.2
	C-1-b	42.5	
	C-1-c	43.5	
Batch-2	C-2-a	6293	42.9
	C-2-b	43.4	
	C-2-c	42.6	
Batch-3	C-3-a	43.2	43.0
	C-3-b	42.2	
	C-3-c	43.5	

4.3 Steel Material Test

4.3.1 Coupon Test

Standardized samples of each of the two steel tubes used to confine the concrete were carefully collected from each throughout the experimental testing phase. These samples were subjected to loading rates of 50 mm/min during the testing process. From the data collected during these tests, engineering stress and engineering strain values were computed to characterize the material behavior.

It is worth noting that, in the notation used, "t1" and "t2" denote the different steel tube thicknesses of 1 mm and 2 mm, respectively. It is important to emphasize that the material properties of these two distinct steel tubes were found to be nearly identical under the same strain rate conditions. Therefore, it is reasonable to assume that these two steel tubes exhibit quite similar material properties.

Table 4. 2 Coupon Test Result

S.No	Specification	Stress Mpa	Strain mm/mm
Series-1	t_1-1	318	0.0137
	t_1-2	351	0.0144
	t_1-3	331	0.0147
Series-2	t_2-1	346	0.0229
	t_2-2	367	0.0237
	t_2-3	358	0.0219

Figure 4.2 illustrates one of the coupon samples that underwent testing under low strain rate conditions. As anticipated, the failure of all the samples transpired within the gage length section of the specimen, which resulted from a reduction in the cross-sectional area. Furthermore, all the samples displayed a satisfactory degree of necking just before reaching the point of rupture.

It is noteworthy that there was an isolated occurrence where one of the samples (t1-2) slipped from the grips of the testing machine during the test. Consequently, this specific test had to be repeated. The slippage incident happened because the grip areas of the specimens were initially manufactured based on standard sizes, but it was later determined that the available grips on the testing machine were slightly smaller in size.

Figure 4. 2 Coupon Test Specimen

4.4 CFDST Test Result

A compressive test is conducted to evaluate the strength and response of CFDST columns when subjected to axial loads. During this test, a CFDST column is subjected to axial compression using a compression testing machine until it eventually fails. The results of this test include the maximum load-bearing capacity, deformation characteristics of the column, and the specific mode of failure observed. In the context of this research, two distinct sets of samples were carefully prepared. One group of samples was dedicated to studying the behavior of specimens equipped with shear connectors positioned on the inner surface of the outer steel tube and the outer surface of the inner steel tube. These specimens were compared to samples without shear connectors. The remaining specimens were designated for investigating the effect of reinforcing the outer steel tube under various conditions.

4.5 Composite tube with shear connector

The comparison between the CFDST Column without shear studs and the specimens having shear studs will be discussed here. In a compressive test of a CFDST column with shear studs on the tubes, the column is loaded vertically until failure occurs. The compressive strength of the column is measured by dividing the maximum load the column can withstand before failure by the cross-sectional area of the column. The test result is

typically reported as the ultimate compressive strength, which is the highest load the column can withstand before failure occurs.

Table

Table 4.3. C-WSC & C-SC (Shear Studs Results)

Specimens	Do x To	Fc (Mpa)	Ductility	Max Load (KN)
C-WSC	152.4 x 1	43.2	3.96	635.27
C-SC	152.4 x 1	43.2	6.50	747.47

The use of shear studs on the tubes helps to enhance the interaction between the concrete and steel tubes, thereby increasing the column's strength and stiffness. The use of shear studs on the tubes can significantly enhance the compressive strength and stiffness of CFDST columns. This is because the shear studs help to transfer the shear stresses between the concrete and steel tubes, thereby enhancing the interaction between them. This interaction results in a more efficient use of the material, leading to increased strength and stiffness of the column.

Failure mode of both column were very different from each other. The CFDST Column having no shear studs fail with a sound and suddenly load become decrease. During load a small fracture occur in the outer steel tube which extend throughout the column and the crack area show that the outer steel tube is completely slip from the concrete. In column having shear studs on the inner side of outer steel tube the failure mode are ductile. When crack occur on top of steel tube but the crack did not extend throughout the column because at every location the steel tube are connected with concrete. The shear studs prevent the propagation of crack in outer steel tube. So the CFDST column having shear studs show ductile behavior than the CFDST column having no shear studs.

Figures 4.3 illustrate the experimental load (N) versus deformation curves for both CFDST columns: one with shear studs and the other without. In this section, we will explore the influence of different parameters on the initial stiffness and ductility behavior of these

tested CFDST columns. Upon a detailed analysis of the figures, it becomes apparent that the presence of shear studs has a negligible impact on the ductility of the columns. Intriguingly, the graphs suggest that the specimens equipped with shear studs display a more ductile behavior when compared to those without shear studs.
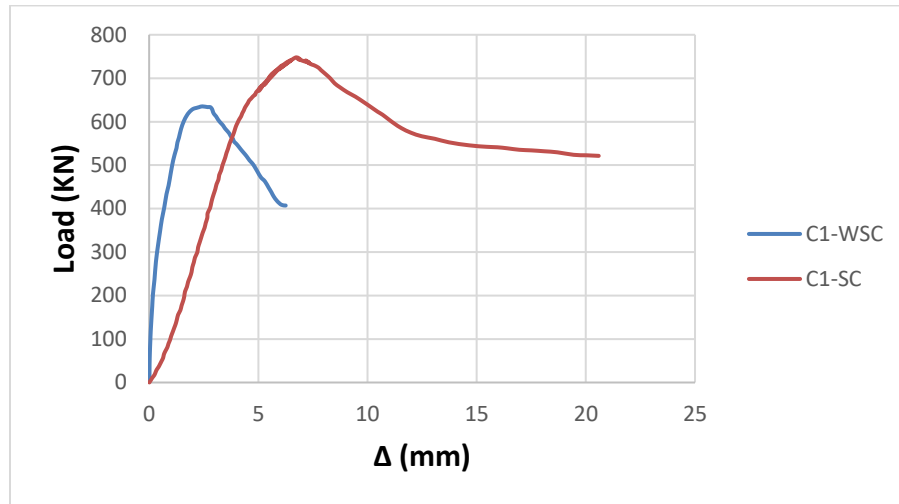

Figure 4. 3 Axial Load VS Δ (mm) Graph of C-WSC & C-SC

Figure 4.3 illustrates a significant drop in the graph of C-WSC, which represents a concrete-filled double-skin tube (CFDST) column without shear studs. Such a sudden drop in the graph of a CFDST column without shear studs could indicate a failure mode commonly referred to as "local buckling." Local buckling occurs in thin-walled structural elements when the compressive stresses within the element exceed a critical limit, causing the wall to buckle outward. This phenomenon reduces the overall stiffness and load-carrying capacity of the structure.

The absence of shear studs in the CFDST column makes it more susceptible to local buckling because there is a lack of lateral restraint on the steel skin. This lack of restraint allows for greater deformation and can lead to a sudden reduction in the load-carrying capacity of the column. The specific location of the sudden drop in the graph can provide insights into the location and extent of the local buckling, shedding light on the overall behavior of the column under load. It is important to note that local buckling is just one of

several potential failure modes that could result in a sudden drop in the load-displacement graph of a CFDST column.

4.6 Control Mix (C1-1mm and C2-2mm)

4.6.1 C1-1mm (1mm Wall Thickness)

In C1-1mm the overall thickness of the inner and outer steel tube were 1mm. This sample were considered as control mix. There is no extra stirrup in the outer steel tube of this sample. In C1-1mm column having shear studs on the inner side of outer steel tube.

4.6.1.1 Failure mode

The failure mode are ductile. When crack occur on top of steel tube but the crack did not extend throughout the column because at every location the steel tube are connected with concrete. The shear studs prevent the propagation of crack in outer steel tube. So the C1-1mm column having shear studs show ductile. The failure mode for this sample is buckling. The steel tube buckle mainly at the mid portion and also at the bottom due to compressive forces, causing the column to fail. This can happen if the applied load is too high, or if the column is too slender. It can be found that local buckling of outer steel tube occur which is a common failure mode in CFDST columns. Local buckling is caused by compressive stresses that exceed the elastic limit of the steel. In all these specimens there is no slippage between steel and concrete due to shear connector.
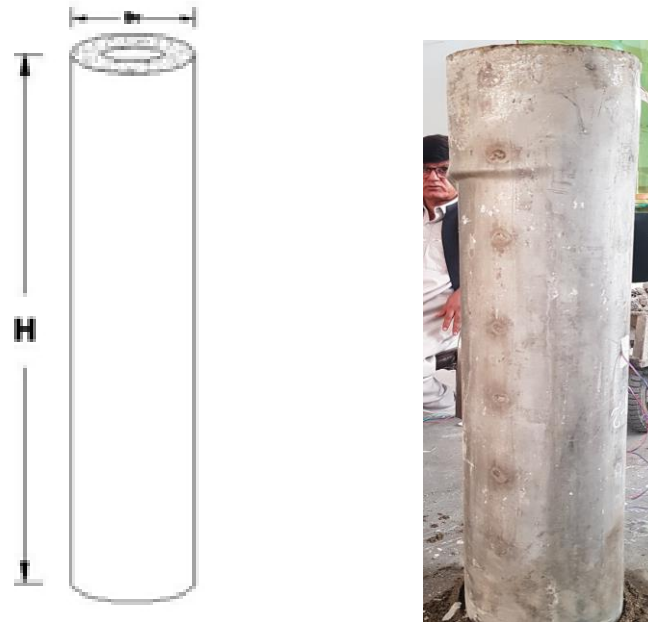
Figure 4. 4 Failure Mode of C1-1mm

Figure 4.4 displays the load versus deformation curves for the tested C1-1mm columns. This section delves into an examination of how various parameters impact the initial stiffness and ductility behavior of these columns. It becomes evident that the yield stress of the outer steel tube has a negligible impact on the initial stiffness of the columns. However, two other factors, namely the wall thickness of the outer tube skin and the grade of concrete used, have distinct effects on the initial stiffness. The load versus axial strain graph of a CFDST column illustrates the relationship between the applied load and the resulting axial strain, which measures the deformation of the column in the axial direction. This behavior typically exhibits nonlinearity and can be divided into multiple stages. In the elastic stage, the column behaves elastically, meaning that the axial strain is directly proportional to the applied load. The slope of the graph in this stage is known as the elastic modulus of the column. As the load increases, the steel tube in the C1-1mm column begins to yield, resulting in a gradual increase in axial strain. The maximum load borne by this column is approximately 760KN. This stage is characterized by a plateau in the

load-axial strain graph. After the yielding stage, the load-axial strain curve continues to increase until the column ultimately fails. The post-yielding stage is typically characterized by a significant decrease in stiffness, as the steel tube has already yielded, and the remaining load is primarily carried by the concrete in the column.
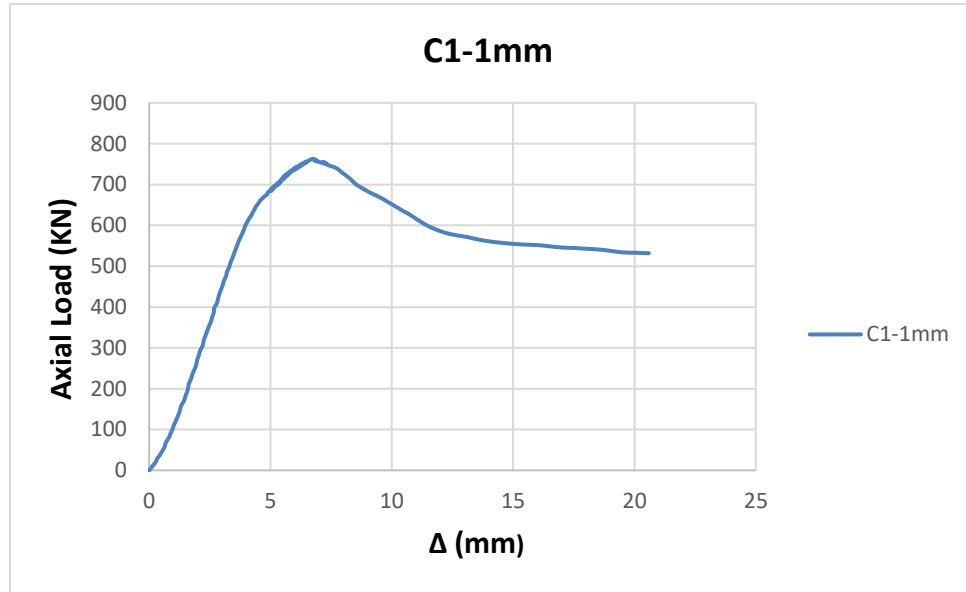

Figure 4. 5 Load VS Strain Graph of CFDST-3

The interaction of the steel skin and concrete core of a C1-1mm column is crucial for load resistance, in part because shear studs are present on the inner side of the outer steel tube. These shear studs play a crucial role in enhancing the load-carrying capacity of a concrete-filled double skin tube (CFDST) column like C1-1mm, reducing the risk of sudden failure due to local buckling or other structural instability modes. Shear studs are typically steel connectors that are welded to the inner surfaces of the steel skin and extend into the concrete core. Their primary function is to facilitate the transfer of shear forces between the steel and concrete components, thereby increasing the overall stiffness and strength of the column. By incorporating shear studs, the C1-1mm column demonstrates improved resistance to local buckling and other potential failure modes. This enhancement results in a more gradual and predictable response under load, reducing the likelihood of

experiencing a sudden drop in the load-displacement curve. The strain gauge located at the top of the column measures the strain in the steel tube's upper section. As depicted in the graph, the strain in this gauge begins to increase gradually as the load is applied, signifying the initial elastic behavior of the steel tube. At a certain point, the strain undergoes a rapid increase, indicating that the steel tube has reached its yield point and is entering the phase of plastic deformation. As the load continues to rise, the strain in the steel tube reaches its maximum value, indicating the failure of the steel tube.
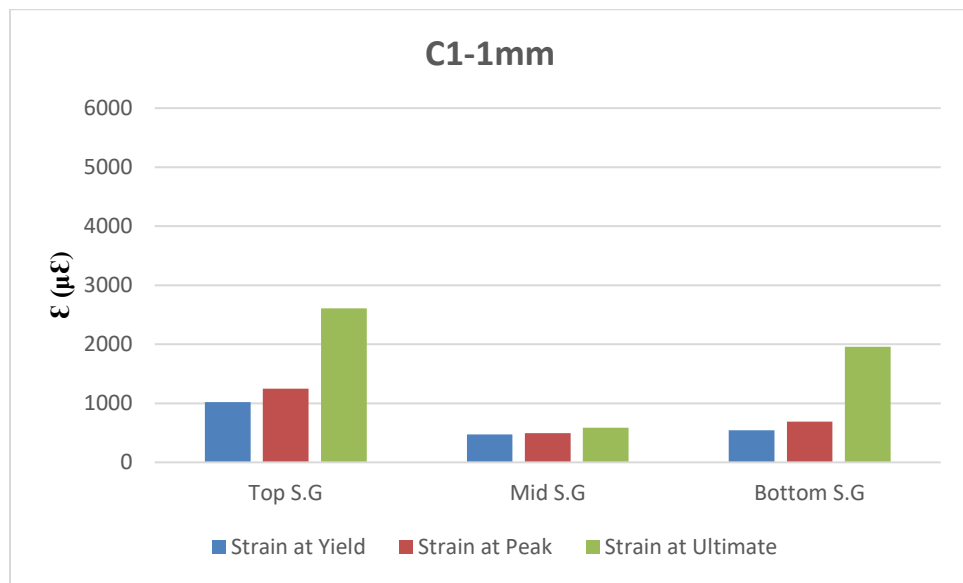

Figure 4. 6 Strain Value at different location of C1-1mm

The strain gauge at the mid is measuring the strain in the steel tube at the middle of the CFDST column. As seen from the graph, study focuses on three key loading stages: the yield point, peak load point, and ultimate point. The primary objective is to investigate and comprehend how strain values evolve at different locations within the column during these critical phases. At the yield point, the column is initially deforming within its elastic range. Strain values at this stage typically exhibit proportionality to the applied load. Analysis of the data indicates that, at this stage, the strain values at all three gauge locations (top, middle, and bottom) were relatively similar. As the column approaches the peak load point, there is an increase in strain values at all gauge locations. Notably, it was observed that the strain gauge at the top of the column recorded significantly higher strain values

compared to the middle and bottom gauges. This observation suggests the possibility of non-uniform deformation within the column, which may be attributed to various factors such as bending effects or localized stress concentrations. At the ultimate point, when the column is nearing or has reached failure, strain values for all three gauge locations registered their highest values. While the top strain gauge continued to record the highest strain.

4.6.1.2   C2-2mm (2mm Wall thickness)

In the case of C2-2mm, both the inner and outer steel tubes had an overall thickness of 2mm. This sample served as the control mix for the study. Unlike C1-1mm, there were no additional stirrups in the outer steel tube of this sample. C2-2mm featured shear studs on the inner side of the outer steel tube. It's important to note that C1-1mm and C2-2mm were considered the control mix samples against which the results of the remaining samples were compared. These control mix samples provided a baseline for evaluating the performance of the other variations in the study.

4.6.1.3   Failure Mode

The load (N) versus deformation curves of C2-2mm were illustrated in this Fig.4.11 The maximum load bear by this column is 959.5KN. Which is about 27% more than that of C1-1mm. All the column from the series 2 will be compare with the series 1 and series-3

The section discussed the ductility behavior of the tested C2-2mm columns. In the load versus deformation graph of a C2-2mm (Concrete Filled Double Skin Tubular) column, the relationship between the applied load and the resulting axial strain (either elongation or compression) of the column is depicted. Fig. 4.11 illustrates this relationship. Axial strain measures the deformation of the column in the axial direction. The load-deformation behavior of a C2-2mm column typically follows a nonlinear pattern and can be divided into several stages. In the elastic stage, the column behaves elastically, meaning that the axial strain is directly proportional to the applied load. The slope of the graph in this stage represents the elastic modulus

45

of the column. As the load continues to increase, the steel tube in the CFDST-8 column begins to yield, leading to a gradual increase in axial strain.
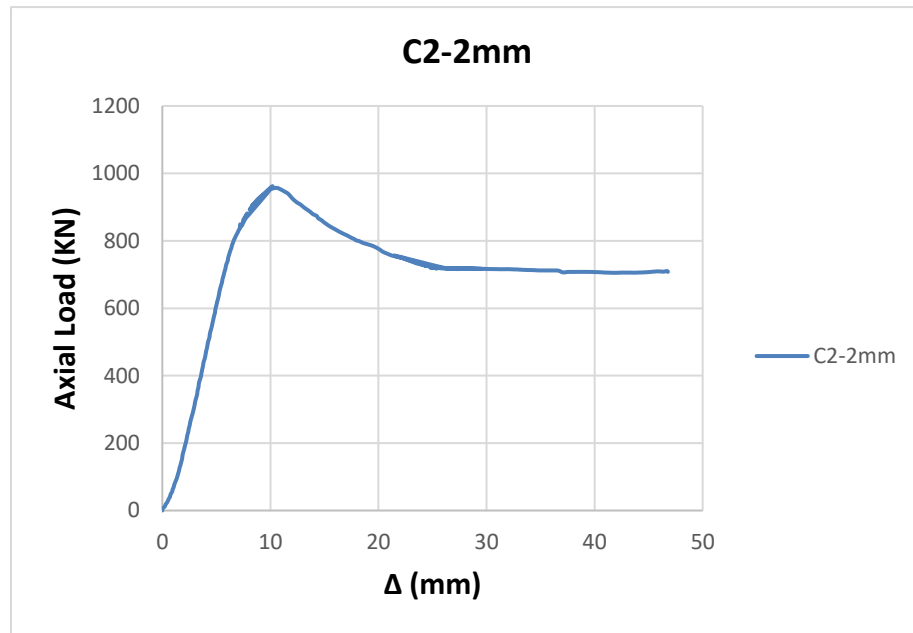

Figure 4. 7. Axial Load V/S Δ (mm) of C2-2mm

The maximum load bear by this column is approximately 960KN. This stage is characterized by a plateau in the load-axial strain graph. After the yielding stage, the load-axial strain curve will continue to increase until the column ultimately fails. The post-yielding stage is typically characterized by a significant decrease in stiffness, as the steel tube has already yielded and the remaining load is carried primarily by the concrete in the column.

Because of the shear studs on the inner side of the outer steel tube, the concrete core and steel skin of a C2-2mm column work together to withstand the loads. The steel skin's strain is measured by the strain gauges, and this information may be utilized to calculate the material's stress and the resulting load on the column. As the load is dispersed uniformly down the length of the column, the gauges' measurements of strain ought to be fairly constant. Shear studs can greatly boost the load-bearing capacity of a concrete filled double skin tube (C2-2mm) column and decrease the risk of unexpected collapse brought on by local buckling or other types of structural instability. Shear studs are normally steel connectors that extend into the concrete

46

core and are welded to the inside surfaces of the steel skin. They contribute to the shear force transfer between the steel and concrete, enhancing the column's overall stiffness and strength. The C2-2mm column will be more resistant to local buckling and other modes of failure with the inclusion of shear studs, which can result in a more gradual and predictable behavior under load.
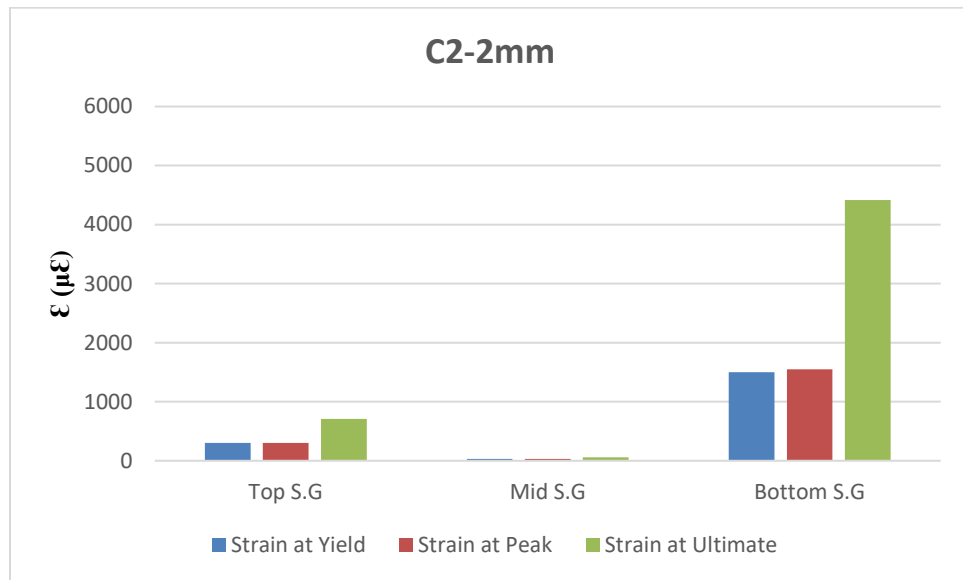

Figure 4. 8. Strain value at different location of C2-2mm

Our investigation focuses on three pivotal loading stages the yield point, the peak load point, and the ultimate point. The primary objective is to gain insights into how strain values evolve at different vertical positions within the column during these critical phases. At yield stage, the strain values at the top and middle gauge locations exhibited relative similarity, while the strain value recorded at the bottom gauge was noticeably higher. Approaching the peak load point, there is an overall increase in strain values at all gauge locations, in line with the anticipated behavior. However, a significant deviation is observed; the strain value recorded at the bottom gauge far surpasses those registered at both the top and middle gauges. As the column nears or reaches its ultimate point, with failure imminent or realized, all gauge locations display their highest strain values. Remarkably, the bottom gauge continues to record the highest strain, emphasizing its distinctive behavior throughout the loading stages.

4.7   Strengthening of Outer Steel Tube

For the purpose of stabilizing the outer steel tube by increasing the thickness of the critical zone of the outer steel tube rather than increasing the overall thickness. In C1-1mm the overall thickness of the inner and outer steel tube were 1mm. This type of sample would be considered as control mix. C1-Do having extra stirrup of width Do/2 at top, bottom, and Do at the center of the Column. At C1-1.5Do having extra stirrup of width Do/2 at top, bottom, and 1.5Do at the center of the Column. At C1-2Do having extra stirrup of width Do/2 at top, bottom, and 2Do at the center of the Column. At C1-Do/2 having extra stirrup of width Do/2 throughout the span of the column. C2-2mm having double outer wall thickness to C1-1mm, which become 2mm. The last two sample of both series will be compare with the above sample. This comparison would tell us about the strengthening of the critical zone only to increasing the whole thickness of the tube.

Series	Specimens	Do x To	Fc (Mpa)	Ductility	Max Load (KN)	%age Increase
Series-1	C1-1mm	152.4 x 1	43.2	3.39	762.19	0
Series-2	C1-Do	152.4 x 1	43.2	7.94	815.16	7.95
	C1-1.5Do	152.4 x 1	42.9	9.91	852.81	12.85
	C1-2Do	152.4 x 1	42.9	12.94	915.84	19.21
	C1-Do/2	152.4 x 1	43.2	6.61	902.57	19.20
Series-3	C2-2mm	152.4 x 2	42.9	4.70	959.52	27.81

4.7.1   C1-1Do (Do at the center)

In C1-1Do having extra stirrup of width Do/2 at top, bottom, and Do at the center of the Column. In this specimen the overall thickness of the outer steel tube is 1mm and at the top (Do/2), Bottom (Do/2) and mid (Do) an extra tube of thickness 1mm is provided. The

result of this sample will be compared with C1-1mm having the outer tube overall thickness is 1mm and C2-2mm having the outer wall thickness of 2mm.

4.7.1.1 Failure Mode

In the case of C1-Do specimens, it's noteworthy that they displayed varying degrees of shear failure when observed from a frontal perspective, primarily characterized by concrete crushing. Shear failure in a concrete-filled double skin short tubular column takes place when the shear stress within the column surpasses the shear resistance capacity of the concrete and steel components. The length of the column, the tensile strength of the concrete infill, and the thickness and strength of the steel tubes are some of the variables that affect the column's resistance to shear failure. Throughout the test, the column experienced outward plastic deformation at various points along its longitudinal axis, which often appeared as diagonal shear failure in the concrete. This type of failure became more pronounced towards the upper part of the column. The inner steel tubes in the examples, as opposed to the infilled concrete, showed essentially little distortion.

Figure 4. 9. Failure Mode of CFDST-4

4.7.1.2 Load versus deformation relationship

Figure 4.10 shows the experimental load (N) vs deformation curves. We will investigate how different parameters affect the initial stiffness and ductility behavior of the tested CFDST columns in this section. According to Figure 4.10, the outer steel tube's yield stress has very little of an effect on the initial stiffness of the columns. On the other hand, the concrete grade and the wall thickness of the outer tube skin have distinct influence on the initial stiffness. Notably, for the C1-Do sample, there is a noticeable greater strain drop compared to the other two samples. Conversely, in the case of C1-Do, the strain drop is minimal at the later stage of deformation.
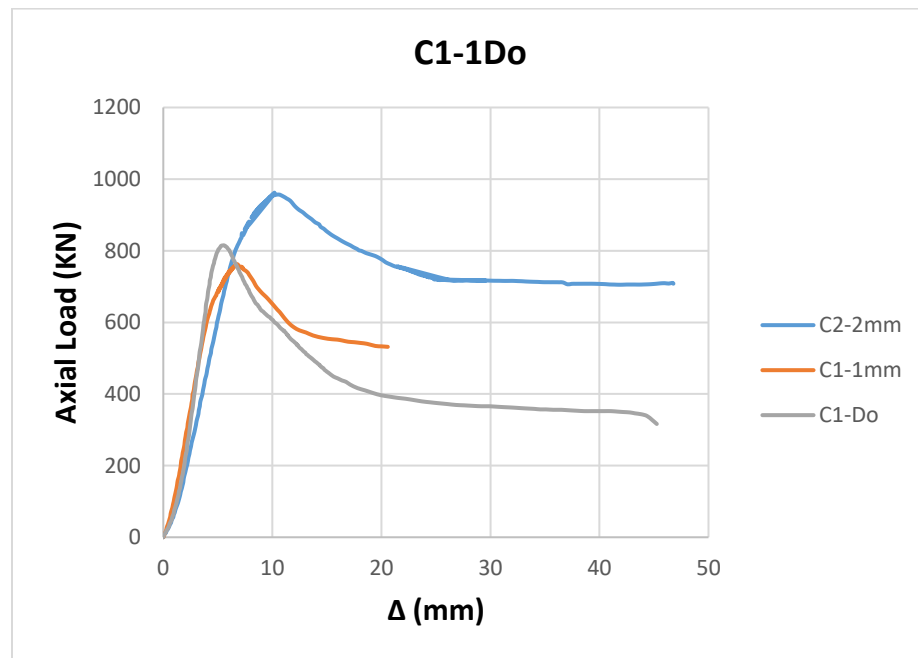
Figure 4. 10. Load VS Δ (mm) of C1-Do

In the elastic stage, the load-axial shortening relationship for all three CFDST columns closely resembles that of a bare steel tube. The axial stiffness of the column is primarily determined by the steel tube, and there is minimal deformation in the concrete core. However, during the post-yield stage, the relationship between load and axial shortening for CFDST columns is influenced by the interaction

between the steel tubes and the concrete core. As the steel tube begins to yield, the concrete core begins to bear a portion of the load. Consequently, the axial stiffness of the column decreases, and the axial shortening increases. In the ultimate stage, the load-axial shortening relationship for C1-Do short columns is dominated by the crushing of the concrete core. At this point, the steel tubes have yielded, and the concrete core has reached its compressive strength limit. The load-carrying capacity of the column is primarily determined by the strength of the concrete core. To provide specific load-bearing values, C1-1mm can bear a maximum load of 755 KN, C1-Do can bear a maximum load of 815 KN, and C2-2mm can withstand a maximum load of 960 KN.

The stiffness of a column can be quantified by the slope of the axial load versus axial strain curve. From the graph, it appears that C1-Do has the steepest slope, indicating that it is the stiffest material of the three. This means that it takes more force to produce a given amount of strain in the C1-Do column compared to the other two columns. The stiffness of c2-2mm is lower than that of C1-Do, and the stiffness of C1-1mm is the lowest among the three. The strength of a column can be quantified by the maximum load it can withstand before it fails. From the graph, it appears that C2-2mm can withstand the highest load before failure, followed by C1-Do and then C1-1mm. The ductility of a column can be quantified by the amount of axial strain it undergoes after reaching its maximum load. C1-Do, which has mid-span stabilization, shows a more gradual decrease in load-carrying capacity and a higher ductility than C2-2mm, indicating that it can sustain a higher level of deformation before failure. From the graph, it appears that C2-2mm and C1-Do exhibit some amount of post-peak ductility, meaning that they are able to continue to deform to some extent after they reach their maximum load. C1-1mm, on the other hand, appears to fail abruptly after reaching its maximum load, indicating that it is a more brittle material than the other two columns.
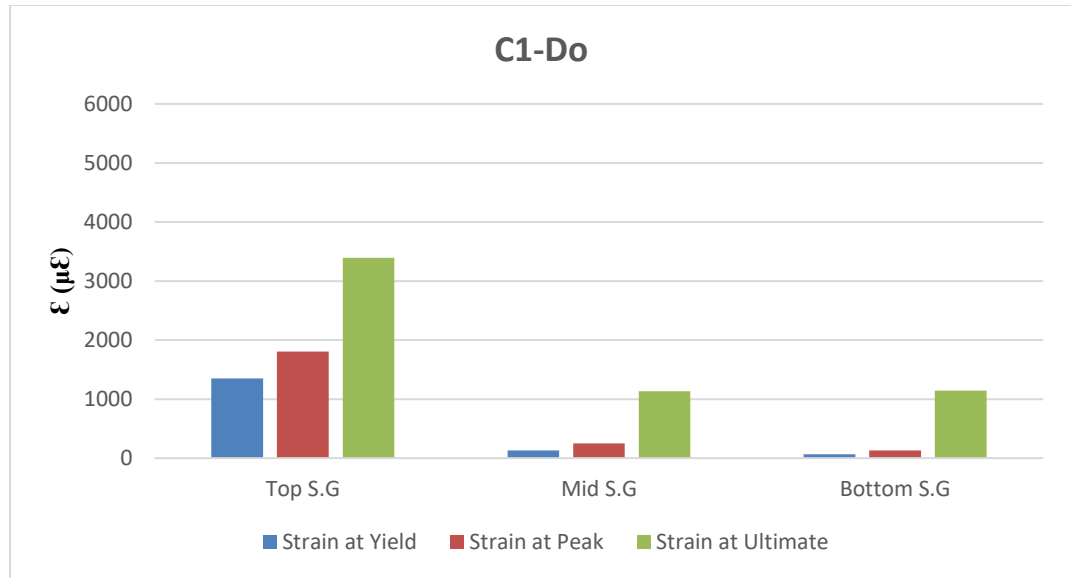
C1-Do

Figure 4. 11. Strain value at different location of C1-Do

The strain gauge at the top of the column has the lowest strain values at lower axial loads, indicating that it experiences the least deformation under smaller loads. However, as the axial load increases, the strain also increases, indicating that the top of the column is beginning to experience deformation. Similarly, the strain gauge at the bottom of the column shows the highest strain values at all loads, indicating that it experiences the highest deformation under load. The strain gauges at the mid-height of the column show intermediate values, with the horizontal strain gauge showing a smaller strain value compared to the vertical strain gauge. The strain gauges installed at the top and bottom of a CFDST (Concrete Filled Steel Tube) column show approximately the same strain value, and the mid-section shows a lower strain value, even though there is extra strengthening provided at the mid-section of the column. The extra strengthening, could have altered the stiffness and strength of the mid-section, leading to a different distribution of the load and hence strain measurements. Depending on the type and location of the strengthening, it could also affect the load transfer mechanism between the steel and concrete in the mid-section, leading to changes in the stress distribution. Due to extra strengthening at the mid portion by Do the ultimate load of the column increased by 10%.

52

4.7.2   C1-1.5Do (1.5-Do at Center)

In C1-1.5Do having extra stirrup of width Do/2 at top, bottom, and 1.5-Do at the center of the Column. In this specimen the overall thickness of the outer steel tube is 1mm and at the top (Do/2), Bottom (Do/2) and mid (1.5-Do) an extra tube of thickness 1mm is provided. The result of this sample will be compared with C1-1mm having the outer tube overall thickness is 1mm and C2-2mm having the outer wall thickness of 2mm.

4.7.2.1   Failure Mode

In the case of C1-1.5Do columns, two common failure modes were observed were the local buckling occurs when compressive stresses exceed the elastic limit of the steel, leading to deformation of the steel tube. Yielding, on the other hand, happens when the axial compressive stress surpasses the yield strength of the steel. In CFDST columns with thinner steel tubes or under high axial stresses, yielding is more probable. The top of the column underwent outward plastic deformation along the longitudinal axis during the test. This plastic deformation is primarily exhibited by the concrete, and the degree of failure becomes more pronounced towards the top of the column. It's worth noting that in all these specimens, there was no slippage between the steel and concrete due to the presence of shear connectors. The inner steel tubes in the examples, as opposed to the infilled concrete, showed essentially little deformation.

Figure 4. 12. Failure Mode of C1-1.5Do

4.7.2.2 Load versus deformation relationship

The load-deformation curves presented in Figure 4.13 provide valuable insights into how different parameters influence the initial stiffness and ductility behavior of the tested CFDST columns. Notably, the data in Figure 4.13 show that the initial stiffness of the columns is only marginally affected by the yield stress of the outer steel tube. However, the initial stiffness is significantly influenced by both the concrete grade and the wall thickness of the outer tube skin. For the C1-1.5Do specimen, it's worth highlighting that after the initial yielding, the load experiences a slight decrease before it begins to increase again. In the cases of both C1-1.5Do and C2-2mm, the strain drop is minimal in the later stages of deformation. This behavior reflects the interaction between the steel tubes and the concrete core as the steel yields and the concrete gradually takes on more of the load-bearing capacity.
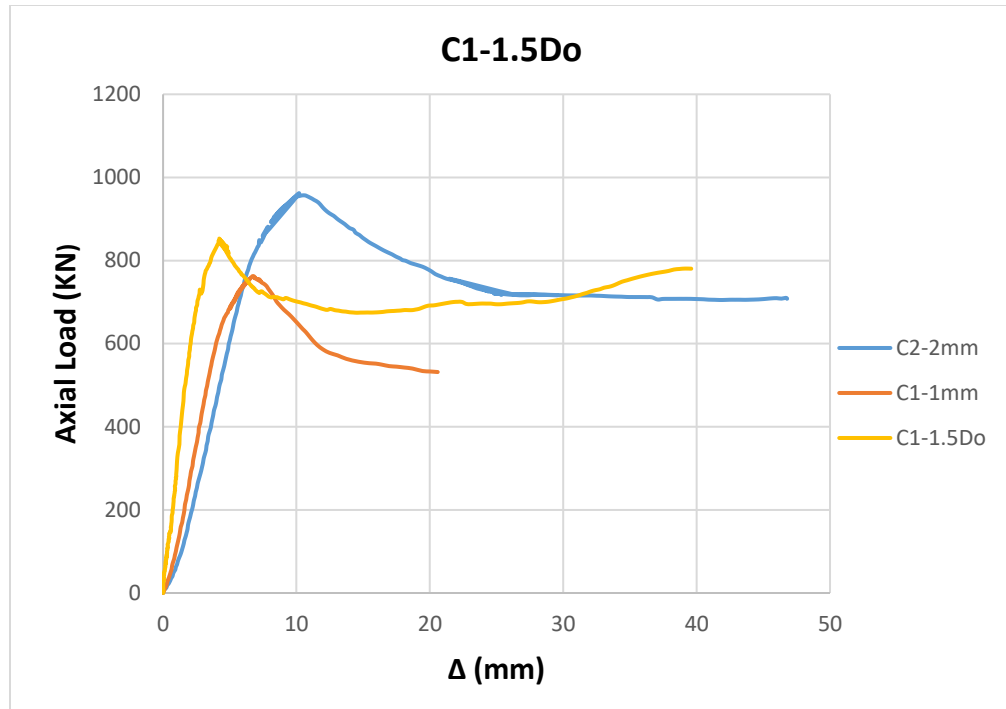
Figure 4. 13. Load V/S Δ (mm) Graph of C1-1.5Do

The load-deformation curves reveal that all three CFDST columns exhibit similar behavior up to a certain point, with a linear increase in axial load corresponding to axial strain. In the elastic stage, the axial load versus deformation graph of C1-1mm, C1-1.5Do, and C2-2mm follows a linear trend. At this stage, the columns behave elastically, with the axial load being directly proportional to the axial strain. The deformation of the concrete core remains minimal during this phase.

As the post-yield stage begins, the axial load versus strain relationship for C1-1.5Do departs from linearity due to the interaction between the steel tubes and the concrete core. During this phase, the steel tubes start to yield, and the axial load is shared between the steel tubes and the concrete core. As a result, the concrete core begins to bear a portion of the load, as illustrated in the figure. Deformation occurs at a slower rate compared to the elastic stage, resulting in a decrease in the axial stiffness of the column. However, as the axial strain continues to increase beyond a certain point, the load-carrying capacity of the columns starts to decline due to factors such as buckling and other failure modes. In the ultimate stage, the axial load versus strain relationship of the specimens exhibits a rapid decrease in axial

stiffness. The concrete core compressive strength has now been exceeded and the steel tubes have started to give way. The strength of the concrete core, which essentially determines the column's ability to carry axial loads, causes axial strain to rise quickly. This behavior marks the ultimate limit state of the column. It's worth noting that C2-2mm exhibits a higher ultimate strength compared to C1-1mm and C1-1.5Do, signifying its ability to withstand a greater axial load before reaching failure. This suggests that increasing the outer wall thickness of the column enhances its ultimate strength. Specifically, C1-1mm can withstand a maximum load of 755 KN, C1-1.5Do can bear a maximum load of 852 KN, and C2-2mm can support a maximum load of 960 KN.
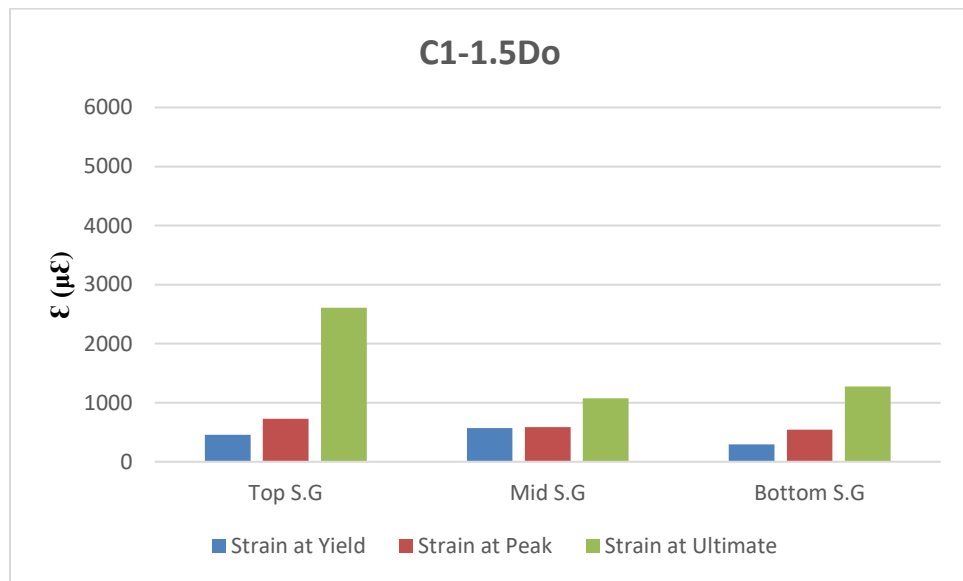
Figure 4. 14. Strain Value at different location of C1-1.5Do

Although a C1-1.5Do has additional reinforcing at the middle, the strain gauges installed at the mid and bottom of the column show roughly the same strain value, and the top of the column shows higher strain value. The additional strengthening may have changed the midsection's stiffness and strength, changing how the load was distributed consequently. The type and position of the strengthening may also have an impact on the system for transferring loads between the steel and concrete in the middle, changing how the stress is distributed. The column's peak load rise

by more than 10% as a result of additional strengthening done in the middle area by 1.5-Do.

4.7.3 C1-2Do (2-Do at center)

In C1-2Do having extra stirrup of width Do/2 at top, bottom, and 2-Do at the center of the Column. In this specimen the overall thickness of the outer steel tube is 1mm and at the top (Do/2), Bottom (Do/2) and mid (2-Do) an extra tube of thickness 1mm is provided. The result of this sample will be compared with C1-1mm having the outer tube overall thickness is 1mm and C2-2mm having the outer wall thickness of 2mm.

4.7.3.1 Failure Mode

In C1-2Do it can be found that local buckling of outer steel tube occur which is a common failure mode in CFDST columns. Local buckling is caused by compressive stresses that exceed the elastic limit of the steel in lower portion of the column. The extra strengthening by 2Do at the mid hold the buckling at the mid. So the stress transfer to the lower portion but it exceed the compressive strength of the C1-2Do which is approximately equal to that of C2-2mm. The yielding of the steel tubes is another failure mode in C1-2Do columns. Yielding in a CFDST column is a consequence of the axial compressive stress surpassing the yield strength of the steel material. This yielding phenomenon is more prone to occur in CFDST columns featuring thinner steel tubes or when subjected to substantial axial loads. The outward plastic deformation primarily manifests at the bottom section of the column, with the concrete core experiencing this outward plastic deformation. This type of failure tends to become more pronounced towards the lower portion of the column. At bottom when steel reach to its yield point the concrete start taking load at that point. The shear studs hold the bond between the steel and concrete due to which there is no slippage occur.

Figure 4. 15. Failure Mode of C1-2Do

4.7.3.2 Load versus Deformation

Figure 4.16 shows the experimental load (N) versus deformation curves, providing insightful information on the effects of different parameters on the initial stiffness and ductility behavior of the tested CFDST columns. As depicted in Figure 4.20, it is evident that the thickness of the outer tube skin and the grade of concrete have a significant impact on the initial stiffness of the columns, whereas the yield stress of the external steel tube has a minimal effect. For C1-2Do, after yielding, the load initially decreases slightly before resuming an increase.

It appears that C1-2Do has the highest load carrying capacity, followed by C2-2mm. Additionally, C1-2Do exhibits the highest stiffness, as evidenced by the steep initial slope of the curve, followed by C2-2mm. In terms of ductility, C1-2Do also appears to exhibit the most ductile behavior, as its curve shows a gradual post-peak decline in load carrying capacity, indicating some degree of energy dissipation capacity. In contrast, C1-1mm and C2-2mm exhibit a more brittle behavior, with a sharp decline in load carrying capacity after reaching the peak value. The maximum

load bear by C1-1mm is 755 KN, while C1-2Do bear maximum load of 905 KN and C2-2mm have maximum load of 960 KN.
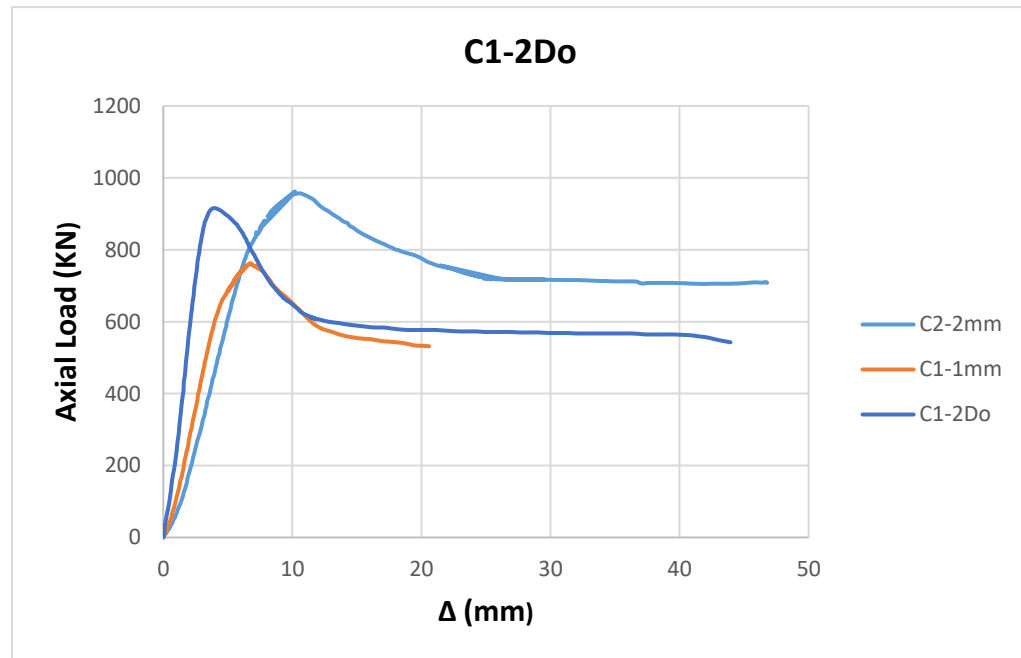
Figure 4. 16. Axial Load V/S Δ (mm) Graph of C1-2Do

The concrete core and steel tubes work together to share the axial weight as the steel tubes start to yield. As seen in fig.4.20, the concrete core begins to carry the load. In comparison to the elastic stage, the axial strain rises more slowly, and the column's axial stiffness decreases. The specimens' axial load versus strain relationship exhibits a rapid decline in axial stiffness in the later stage. The concrete core's compressive strength has been exceeded and the steel tubes have given way. The strength of the concrete core primarily determines the column's ability to bear axial loads, and axial strain rises quickly.

Figure 4. 17. Strain value at different location of C1-2Do
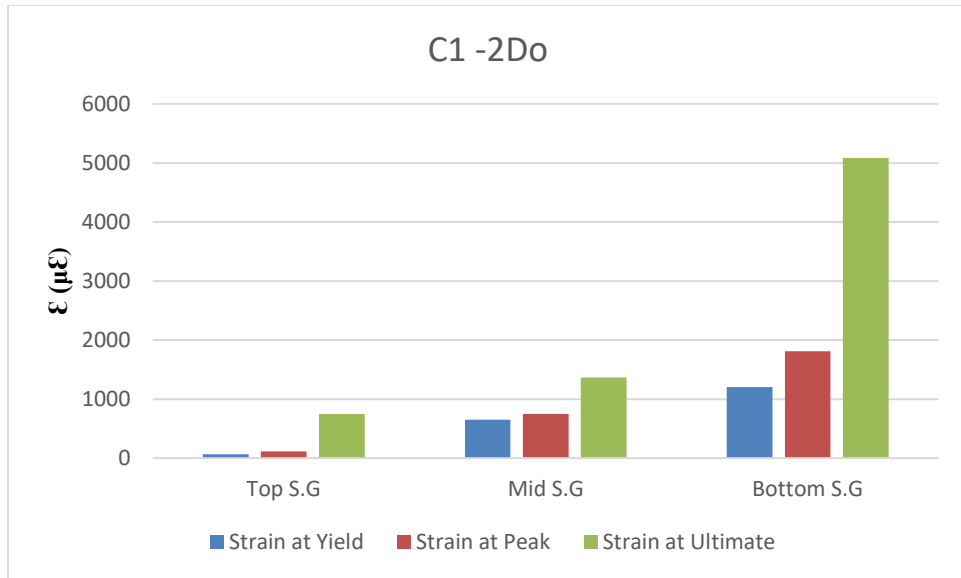
The strain gauge at the top of the column shows a nearly linear increase in strain with increasing axial load, indicating that it experiences a proportional amount of deformation as the load is increased. The strain gauge at the bottom of the column shows a similar linear increase in strain with increasing axial load, but with higher values than the top strain gauge. This indicates that the bottom of the column is experiencing greater deformation under load than the top of the column. The two strain gauges at the mid-height of the column, one horizontal and one vertical, show different behavior. The horizontal strain gauge shows a nearly linear increase in strain with increasing axial load, similar to the top and bottom strain gauges. However, the vertical strain gauge shows a different trend, with an initial linear increase in strain followed by a decrease in strain at higher loads. This may be due to buckling of the steel tube under compressive loads, leading to a reduction in strain as the tube begins to buckle. Despite the addition of additional reinforcing at the middle of the column, the strain gauges installed at the top and bottom of a CFDST (Concrete Filled Steel Tube) column show almost the same strain value, while the midsection displays a lower strain value. The additional reinforcing may have changed the midsection's stiffness and tensile strength, changing how the load was distributed and, consequently, how the strain was measured. The type and placement of the reinforcing may also modify the way that loads are transferred

60

between the steel and concrete in the middle, which could alter how the stress is distributed. The ultimate load of the column increased by 20% as a result of 2-Do additional reinforcing at the middle region.

4.7.4   C1-Do/2 (Do on overall column)

In C1-Do/2 having extra stirrup of width Do/2 from top to bottom of the Column. In this specimen the overall thickness of the outer steel tube is 1mm and at Do/2 distance an extra tube of thickness 1mm is provided. The result of this sample will be compared with C1-1mm and C2-2mm.

4.7.4.1   Failure Mode

Diagonal shear failure, a common mode of failure in CFDST columns, is observed in C1-Do/2. Shear failure in a concrete-filled double skin short tubular column occurs when the shear stress within the column surpasses the shear resistance capacity of the concrete and steel components. This failure mode is characterized by diagonal cracks located at the bottom of the C1-Do/2 short column. The shear resistance of such a column is influenced by several factors, including the thickness and strength of the steel tubes, the strength and stiffness of the concrete infill, and the length of the column.

Figure 4. 18. Failure Mode of C1-Do/2

Yielding of the steel tubes is another failure mechanism observed in C1-Do/2 columns. This type of failure is caused by the axial compressive stress exceeding the yield strength of the steel. It is more likely to occur in CFDST columns with thinner steel tubes or under high axial loads. In a concrete-filled double skin short tubular column, yielding of the outer steel tube occurs when the stress in the outer steel tube reaches its yield strength. This can happen when the applied load exceeds the capacity of the column to resist the load. The outer steel tube provides both axial and flexural strength to the column. When the outer steel tube yields, the column loses its flexural strength and becomes unstable. It may continue to carry the load, but with reduced stiffness and capacity, and may eventually buckle or collapse if the load continues to increase. It is essential to consider all potential failure modes, including axial, flexural, and shear failure, as well as yielding of the outer steel tube, in the design of a concrete-filled double skin short tubular column. The presence of shear studs helps maintain the bond between the steel and concrete, preventing slippage. However, unlike the infilled concrete, the inner steel tubes in the specimens exhibit almost no deformation.

4.7.4.2 Load versus deformation curve

The contours of the experimental load versus deflection are presented in Fig. 4.23. This section discussed the influence of various parameters on the initial stiffness and ductility behavior of the tested CFDST columns. The load versus strain graph for a concrete filled double skin short column will have several distinct stages. Initially, all the three column behave elastically, with the load increasing linearly with strain. This stage is known as the elastic range. At this stage the C1-1mm, C1-Do/2 and C2-2mm has approximately the same behavior. A linear connection exists between the axial load and strain for a C1-1mm, C1-Do/2 and C2-2mm during the elastic stage. The column acts like an elastic member, and the relationship between the axial load and the axial strain is linear. Concrete core displacement is hardly noticeable at this point. The maximum load bear by C1-1mm is 755 KN, while C1-Do/2 bear maximum load of 902 KN and C2-2mm have maximum load of 960 KN. Thus it show that the C1-2Do and C1-Do/2 approximately bear the same load.
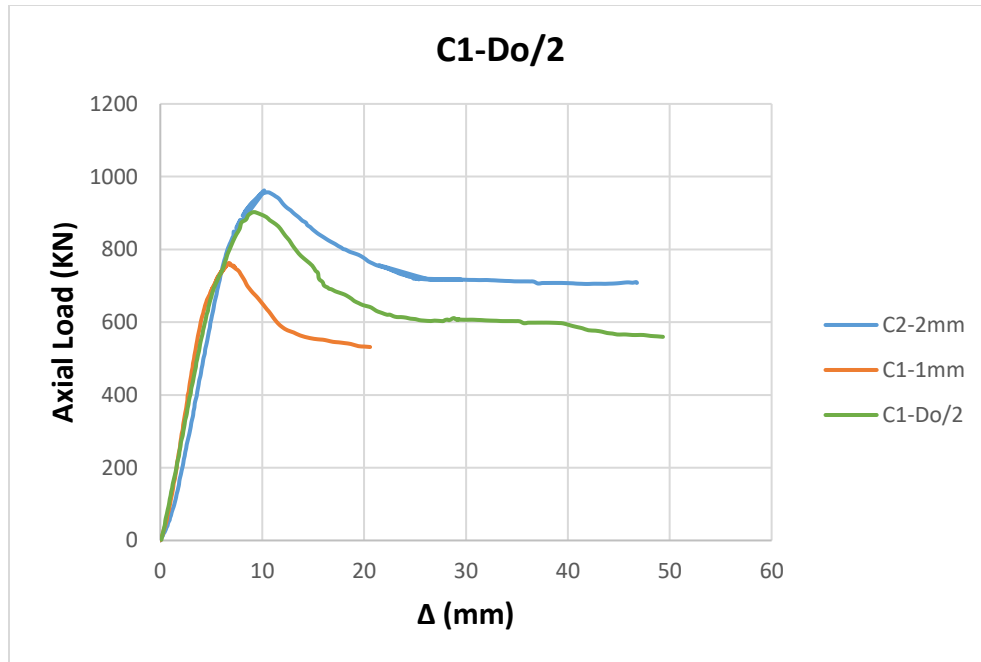
C1-Do/2

Figure 4. 19. Axial Load V/S Δ (mm) Graph of C1-Do/2

As the load on the column increases, it will eventually reach its yield point, where the column begins to deform plastically as shown in fig.4.23. At this point, the load will continue to increase, but the deformation will increase at a faster rate than before. The load on the column continues to increase beyond the yield point, the column begins to deform more rapidly and eventually reach a point where it can no longer support the load, known as the ultimate load. In terms of strength, C2-2mm also has the highest ultimate strength, followed by C1-Do/2, and then C1-1mm. This is expected, as the thicker outer wall of C2-2mm would be able to resist higher loads before failure. In terms of ductility, C1-Do/2 shows the highest ductility among the three, with the highest strain capacity before failure. This may be due to the extra sheet providing additional stability and support throughout the column, allowing for more deformation before failure.
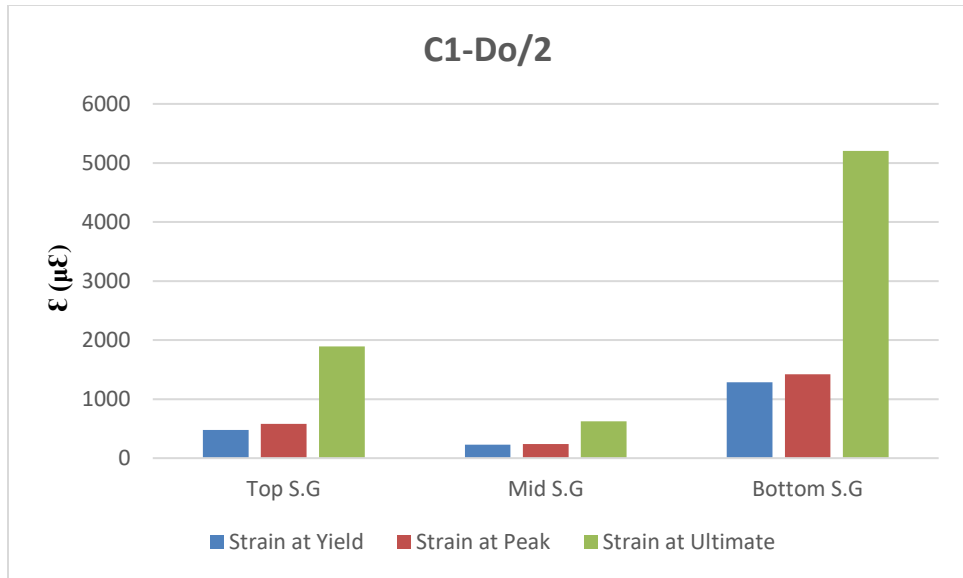
Figure 4. 20. Strain value at different location of C1-Do/2

In Fig.4.24, discussing the bar chart that represents the strain values in the CFDST C1-D0/2 column at different loading stages, including the yield point, peak load point, and ultimate point. To analyze the strain values in the CFDST C1-D0/2 column effectively, we need to consider three significant loading stages. The yield point is the stress level at which the material begins to exhibit permanent deformation. Strain values at this stage are crucial because they indicate when the column starts to deform plastically. At the peak load point, the column reaches its maximum load-bearing capacity before experiencing a decline. Strain values here provide insights into the column's peak performance. The ultimate point represents the point at which the column can no longer support the load and undergoes structural failure. Understanding strain values at this stage is crucial for assessing the column's safety margin. The bottom section of the column bears the most significant load. Consequently, the strain experienced at the bottom is higher due to the increased stress concentration.

CONCLUSIONS AND RECOMMENDATIONS

5.1. Conclusions

Four CFDST columns, incorporating shear connectors to enhance the interaction between the steel and concrete elements, were subjected to axial compressive loads. These externally confined CFDST columns were then evaluated and compared to unconfined CFDST columns in terms of their axial load-carrying capacity, elastic stiffness, and ductility. To optimize the effectiveness of steel tube confinement, various configurations were explored, including different external tube spacings (Do, 1.5Do, and 2Do) and varying column lengths (Do/2).

From the test results, it was observed that

➢ The presence of shear studs in a concrete filled double skin tube (C-SC) column can significantly increase its load-carrying capacity as compared to C-WSC and reduce the likelihood of sudden failure due to local buckling or other modes of structural instability. Without shear studs, the CFDST column is more susceptible to local buckling due to the lack of lateral restraint on the steel skin, which can lead to a sudden reduction in the load-carrying capacity of the column.

➢ The results clearly demonstrate that shear studs significantly improve the load-carrying capacity of these columns. In fact, the load-carrying capacity was observed to increase by an impressive 15.2% when compared to C-WSC columns. This remarkable improvement is attributed to the enhanced load transfer mechanism facilitated by shear studs, creating a robust bond between the concrete core and the outer steel tube.

➢ It was observed that increasing the wall thickness of the outer steel tube and elevating the yield stress at the critical area of the tube further enhance the bearing capacity and ductility of the column. These structural enhancements work synergistically with the presence of shear studs to create a robust, high-capacity, and ductile structural element that can effectively withstand both applied loads and potential lateral displacements.

➢ The incorporation of extra strengthening measures on the outer steel tube of CFDST short columns has yielded significant improvements in their load-carrying capacity when

compared to the control mix. The findings of this study underscore the importance of these enhancements in enhancing the structural performance of such columns.

➢ Addition of extra strengthening to the outer steel tube can result in an impressive increase in the maximum load-carrying capacity, ranging from 10% to 20% in comparison to the control mix. This substantial improvement is a testament to the effectiveness of the strengthening measures in augmenting the structural capacity of CFDST short columns.

➢ The study has elucidated a crucial relationship between the load-carrying capacity and the level of confinement provided to the outer steel tube. As the confinement of the outer steel tube increases, it leads to a larger confining pressure exerted on the concrete infill. This elevated confinement effect directly contributes to the observed enhancements in load-carrying capacity. This phenomenon highlights the significance of proper confinement measures in the design and construction of CFDST short columns.

5.2. Recommendations

The following steps could be done to carry out more study, address some of the problems, and raise the standard of the predictions made by the experimental program.

- To build upon this study's findings, further exploration can be conducted to investigate additional aspects of CFDST columns, such as their response to lateral, torsional, or dynamic loads

- Exploring alternative materials, designs, or treatments that can boost the strength of the outer steel tube without increasing its overall thickness remains a viable research avenue.

- Assessing CFST samples under higher loading rates can provide valuable insights into their behavior when subjected to impact or dynamic loading conditions,

- Utilizing a displacement-controlled loading mode during testing offers the potential for a more precise depiction of post-ultimate behavior, allowing for a comprehensive understanding of ductility and energy absorption.nhancing their applicability in real-world scenarios.

REFERENCES

A. (2013). "CT-13 ACI Concrete Terminology." ACI Materials Journal.

Abeer, S., et al. (2020). "Investigation some properties of recycled lightweight concrete blocks as a fine aggregate in mortar under elevated temperature." Periodicals of Engineering and Natural Sciences (PEN) **8**(1): 400-412.

Akca, A. H. and N. Ö. Zihnioğlu (2013). "High performance concrete under elevated temperatures." Construction and Building Materials **44**: 317-328.

Al-Akhras, N. M., et al. (2009). "Performance of olive waste ash concrete exposed to elevated temperatures." Fire Safety Journal **44**(3): 370-375.

Ali, F., et al. (2001). "Explosive spalling of high-strength concrete columns in fire." Magazine of Concrete Research **53**(3): 197-204.

Anderberg, Y. (1997). Spalling phenomena of HPC and OC. NIST Workshop on Fire Performance of High Strength Concrete in Gaithersburg.

Aseem, A., et al. (2019). "Structural health assessment of fire damaged building using non-destructive testing and micro-graphical forensic analysis: A case study." Case Studies in Construction Materials **11**: e00258.

Astm, A. (2015). "C617/C617M 15–standard practice for capping cylindrical concrete specimens." ASTM American Society for Testing and Materials–Committee C09 on Concrete and Concrete Aggregates–Subcommittee C **9**.

ASTM, A. (2017). "C150/C150M-17, Standard Specification for Portland Cement." American Society for Testing and Materials: West Conshohocken, PA, USA.

Awal, A. A., et al. (2015). "Effect of cooling regime on the residual performance of high-volume palm oil fuel ash concrete exposed to high temperatures." Construction and Building Materials **98**: 875-883.

Bamigboye, G., et al. (2021). "Mechanical and durability assessment of concrete containing seashells: A review." Cogent Engineering **8**(1): 1883830.

Barnett, S., et al. (2004). "Fast-track concrete construction using cement replacement materials." Special Publication **221**: 135-152.

Bastami, M., et al. (2011). "Performance of high strength concretes at elevated temperatures." Scientia Iranica **18**(5): 1028-1036.

Bažant, Z. P., et al. (1996). "Concrete at high temperatures: material properties and mathematical models."

Bijen, J. (1996). "Blast furnace slag cement for durable marine structures. Stichting Beton Prima." Amsterdam: Elservier.

C33, A. (2003). "ASTM C33 standard specifications for concrete aggregates." ASTM Standard Book.

C1231/C1231M-12 "A.C.M.-. Practice for Use of Unbonded Caps in Determination of Compressive Strength of Hardened Concrete Cylinders.".

Carino, N. (1994). "Effects of testing variables on the strength of high-strength (90 MPa) concrete cylinders." Special Publication **149**: 589-632.

Castillo, C. (1987). Effect of transient high temperature on high-strength concrete, Rice University.

Castillo, C. and A. Durrani (1990). "Effect of transient high-temperature on high-strength concrete-closure." ACI Materials Journal **87**(6): 653-653.

Chan, Y., et al. (1999). "Residual strength and pore structure of high-strength concrete and normal strength concrete after exposure to high temperatures." Cement and Concrete Composites **21**(1): 23-27.

Chandra, S. and L. Berntsson (2002). Lightweight aggregate concrete, Elsevier.

Cheng, F.-P., et al. (2004). "Stress-strain curves for high strength concrete at elevated temperatures." Journal of Materials in Civil Engineering **16**(1): 84-90.

Committee, A. (2008). Guide for selecting proportions for high-strength concrete using Portland cement and other cementitious materials, American Concrete Institute.

Concrete, A. I. C. C. o. and C. Aggregates (2014). Standard test method for compressive strength of cylindrical concrete specimens, ASTM international.

Demir, I., et al. (2011). "Performance of cement mortars replaced by ground waste brick in different aggressive conditions." Ceramics-Silikáty **55**(3): 268-275.

Duval, R. and E. Kadri (1998). "Influence of silica fume on the workability and the compressive strength of high-performance concretes." Cement and Concrete Research **28**(4): 533-547.

Ergün, A., et al. (2013). "The effect of cement dosage on mechanical properties of concrete exposed to high temperatures." Fire Safety Journal **55**: 160-167.

Evart, B. (2018). "Fire Loss In The United State During 2017, Natl. Fire Prot. Assoc. ."

Felicetti, R., et al. (2013). "Thermal and mechanical properties of light-weight concrete exposed to high temperature." Fire and materials **37**(3): 200-216.

Georgali, B. and P. Tsakiridis (2005). "Microstructure of fire-damaged concrete. A case study." Cement and Concrete Composites **27**(2): 255-259.

Han, C.-G., et al. (2005). "Performance of spalling resistance of high performance concrete with polypropylene fiber contents and lateral confinement." Cement and Concrete Research **35**(9): 1747-1753.

Heap, M., et al. (2013). "The influence of thermal-stressing (up to 1000 C) on the physical, mechanical, and chemical properties of siliceous-aggregate, high-strength concrete." Construction and Building Materials **42**: 248-265.

Hoff, G. C., et al. (2000). "Elevated temperature effects on HSC residual strength." Concrete International **22**(4): 41-48.

Hora, M., et al. (2013). "Temperature analysis of lightweight aggregate concrete slab members at elevated temperatures for predicting fire resistance." Applications of Structural Fire Engineering.

Horszczaruk, E., et al. (2017). "The effect of elevated temperature on the properties of cement mortars containing nanosilica and heavyweight aggregates." Construction and Building Materials **137**: 420-431.

Husem, M. (2006). "The effects of high temperature on compressive and flexural strengths of ordinary and high-performance concrete." Fire Safety Journal **41**(2): 155-163.

Janotka, I. and T. Nürnbergerová (2005). "Effect of temperature on structural quality of the cement paste and high-strength concrete with silica fume." Nuclear Engineering and Design **235**(17-19): 2019-2032.

Kalifa, P., et al. (2000). "Spalling and pore pressure in HPC at high temperatures." Cement and Concrete Research **30**(12): 1915-1927.

Khaliq, W. (2012). Performance characterization of high performance concretes under fire conditions.

Khaliq, W. (2018). "Mechanical and physical response of recycled aggregates high-strength concrete at elevated temperatures." Fire Safety Journal **96**: 203-214.

Khaliq, W. and H. A. Khan (2015). "High temperature material properties of calcium aluminate cement concrete." Construction and Building Materials **94**: 475-487.

Khaliq, W. and V. Kodur (2011). "Thermal and mechanical properties of fiber reinforced high performance self-consolidating concrete at elevated temperatures." Cement and Concrete Research **41**(11): 1112-1122.

Khaliq, W. and F. Waheed (2017). "Mechanical response and spalling sensitivity of air entrained high-strength concrete at elevated temperatures." Construction and Building Materials **150**: 747-757.

Khan, E. U., et al. (2020). "Spalling sensitivity and mechanical response of an ecofriendly sawdust high strength concrete at elevated temperatures." Construction and Building Materials **258**: 119656.

Knaack, A. M., et al. (2011). "Compressive stress-strain relationships for North American concrete under elevated temperatures." ACI Materials Journal **108**(3): 270.

Kodur, V. (2000). Spalling in high strength concrete exposed to fire: concerns, causes, critical parameters and cures. Advanced Technology in Structural Engineering**:** 1-9.

Kodur, V. (2014). "Properties of concrete at elevated temperatures." International Scholarly Research Notices **2014**.

Kodur, V., et al. (2013). "An approach to account for tie configuration in predicting fire resistance of reinforced concrete columns." Engineering structures **56**: 1976-1985.

Lankard, D. R., et al. (1971). "Effects of moisture content on the structural properties of portland cement concrete exposed to temperatures up to 500F." Special Publication **25**: 59-102.

Lau, A. and M. Anson (2006). "Effect of high temperatures on high performance steel fibre reinforced concrete." Cement and Concrete Research **36**(9): 1698-1707.

Lertwattanaruk, P., et al. (2012). "Utilization of ground waste seashells in cement mortars for masonry and plastering." Journal of environmental management **111**: 133-141.

Lie, T. and V. Kodur (1996). "Thermal and mechanical properties of steel-fibre-reinforced concrete at elevated temperatures." Canadian Journal of Civil Engineering **23**(2): 511-517.

Lie, T. T. and J. Woollerton (1988). Fire resistance of reinforced concrete columns: test results, National Research Council Canada, Institute for Research in Construction.

Luo, X., et al. (2000). "Effect of heating and cooling regimes on residual strength and microstructure of normal strength and high-performance concrete." Cement and Concrete Research **30**(3): 379-383.

Marar, K., et al. (2001). "Relationship between impact energy and compression toughness energy of high-strength fiber-reinforced concrete." Materials letters **47**(4-5): 297-304.

Marara, K., et al. (2011). "Compression specific toughness of normal strength steel fiber reinforced concrete (NSSFRC) and high strength steel fiber reinforced concrete (HSSFRC)." Materials Research **14**: 239-247.

Martínez-García, C., et al. (2019). "Design and properties of cement coating with mussel shell fine aggregate." Construction and Building Materials **215**: 494-507.

Mazloom, M., et al. (2004). "Effect of silica fume on mechanical properties of high-strength concrete." Cement and Concrete Composites **26**(4): 347-357.

Menzel, C. A. (1943). Tests of the fire resistance and thermal properties of solid concrete slabs and their significance, National Emergency Training Center.

Miura, T. and I. Iwaki (2000). "Strength development of concrete incorporating high levels of ground granulated blast-furnace slag at low temperatures." Materials Journal **97**(1): 66-70.

Naceri, A. and M. C. Hamina (2009). "Use of waste brick as a partial replacement of cement in mortar." Waste management **29**(8): 2378-2384.

Nadeem, A., et al. (2014). "The performance of fly ash and metakaolin concrete at elevated temperatures." Construction and Building Materials **62**: 67-76.

Nassif, A., et al. (1999). "The effects of rapid cooling by water quenching on the stiffness properties of fire-damaged concrete." Magazine of Concrete Research **51**(4): 255-261.

Netinger, I., et al. (2011). "The effect of high temperatures on the mechanical properties of concrete made with different types of aggregates." Fire Safety Journal **46**(7): 425-430.

Nguyen, D. H., et al. (2017). "Durability of pervious concrete using crushed seashells." Construction and Building Materials **135**: 137-150.

Noumowé, A., et al. (2009). "Thermo-mechanical characteristics of concrete at elevated temperatures up to 310 C." Nuclear Engineering and Design **239**(3): 470-476.

Oktay, H., et al. (2015). "Mechanical and thermophysical properties of lightweight aggregate concretes." Construction and Building Materials **96**: 217-225.

Othuman, M. A. and Y. Wang (2011). "Elevated-temperature thermal properties of lightweight foamed concrete." Construction and Building Materials **25**(2): 705-716.

Panda, K. C., et al. (2020). "Effect of rice husk ash on mechanical properties of concrete containing crushed seashell as fine aggregate." Materials Today: Proceedings **32**: 838-843.

Panda, K. C., et al. (2020). Effect of Ground Granulated Blast Furnace Slag on the Properties of Sea Shell Concrete. IOP Conference Series: Materials Science and Engineering, IOP Publishing.

Pašalić, S., et al. (2012). "Pozzolanic mortars based on waste building materials for the restoration of historical buildings." Chemical Industry and Chemical Engineering Quarterly/CICEQ **18**(2): 147-154.

Peng, G.-F., et al. (2008). "Effect of thermal shock due to rapid cooling on residual mechanical properties of fiber concrete exposed to high temperatures." Construction and Building Materials **22**(5): 948-955.

Peng, G., et al. (2001). "Chemical kinetics of CSH decomposition in hardened cement paste subjected to elevated temperatures up to 800 C." Advances in cement research **13**(2): 47-52.

Phan, L. T. (2002). "High-strength concrete at high temperature-an overview." Proceedings of 6th international symposiumon utilization of high strength/high performance concrete, Leipzig, Germany: 501-518.

Phan, L. T. and N. J. Carino (1998). "Review of mechanical properties of HSC at elevated temperature." Journal of Materials in Civil Engineering **10**(1): 58-65.

Phan, L. T. and N. J. Carino (2001). "Mechanical properties of high-strength concrete at elevated temperatures."

Phan, L. T. and N. J. Carino (2002). "Effects of test conditions and mixture proportions on behavior of high-strength concrete exposed to high temperatures." ACI Materials Journal **99**(1): 54-66.

Phan, L. T., et al. (2001). "Effects of elevated temperature exposure on heating characteristics, spalling, and residual properties of high performance concrete." Materials and structures **34**(2): 83-91.

Phan, L. T. and L. Phan (1996). Fire performance of high-strength concrete: A report of the state-of-the art, US Department of Commerce, Technology Administration, National Institute of ….

Poon, C.-S., et al. (2001). "Comparison of the strength and durability performance of normal-and high-strength pozzolanic concretes at elevated temperatures." Cement and Concrete Research **31**(9): 1291-1300.

Poon, C.-S., et al. (2003). "Performance of metakaolin concrete at elevated temperatures." Cement and Concrete Composites **25**(1): 83-89.

Poon, C. S., et al. (2000). "A study on high strength concrete prepared with large volumes of low calcium fly ash." Cement and Concrete Research **30**(3): 447-455.

Poon, C. S., et al. (2004). "Compressive behavior of fiber reinforced high-performance concrete subjected to elevated temperatures." Cement and Concrete Research **34**(12): 2215-2222.

Real, S., et al. (2016). "Contribution of structural lightweight aggregate concrete to the reduction of thermal bridging effect in buildings." Construction and Building Materials **121**: 460-470.

Rizwan, S. A. (2006). "High-performance mortars and concrete using secondary raw materials."

Safi, B., et al. (2011). "Rheology and zeta potential of cement pastes containing calcined silt and ground granulated blast-furnace slag." Materiales de Construcción **61**(303): 353-370.

Safi, B., et al. (2013). "Effect of the heat curing on strength development of self-compacting mortars containing calcined silt of dams and Ground Brick Waste." Materials Research **16**: 1058-1064.

Safi, B., et al. (2013). "The use of plastic waste as fine aggregate in the self-compacting mortars: Effect on physical and mechanical properties." Construction and Building Materials **43**: 436-442.

Safi, B., et al. (2015). "The use of seashells as a fine aggregate (by sand substitution) in self-compacting mortar (SCM)." Construction and Building Materials **78**: 430-438.

Sakr, K. and E. El-Hakim (2005). "Effect of high temperature or fire on heavy weight concrete properties." Cement and Concrete Research **35**(3): 590-596.

Sancak, E., et al. (2008). "Effects of elevated temperature on compressive strength and weight loss of the light-weight concrete with silica fume and superplasticizer." Cement and Concrete Composites **30**(8): 715-721.

Sanjayan, G. and L. Stocks (1993). "Spalling of high-strength silica fume concrete in fire." Materials Journal **90**(2): 170-173.

Shi, C. and K. Zheng (2007). "A review on the use of waste glasses in the production of cement and concrete." Resources, conservation and recycling **52**(2): 234-247.

Sikora, P., et al. (2018). "The effects of Fe3O4 and Fe3O4/SiO2 nanoparticles on the mechanical properties of cement mortars exposed to elevated temperatures." Construction and Building Materials **182**: 441-450.

Standard, A. (2016). "Standard practice for making and curing concrete test specimens in the laboratory." ASTM International.

Toutanji, H., et al. (2004). "Effect of supplementary cementitious materials on the compressive strength and durability of short-term cured concrete." Cement and Concrete Research **34**(2): 311-319.

Varhen, C., et al. (2017). "Experimental investigation of Peruvian scallop used as fine aggregate in concrete." Construction and Building Materials **136**: 533-540.

Xiao, J., et al. (2016). "Effect of strain rate on compressive behaviour of high-strength concrete after exposure to elevated temperatures." Fire Safety Journal **83**: 25-37.

Yang, E.-I., et al. (2005). "Effect of oyster shell substituted for fine aggregate on concrete characteristics: Part I. Fundamental properties." Cement and Concrete Research **35**(11): 2175-2182.

Yu, Z. and D. Lau (2017). "Evaluation on mechanical enhancement and fire resistance of carbon nanotube (CNT) reinforced concrete." Coupled Syst. Mech **6**(3): 335-349.

Zeiml, M., et al. (2006). "How do polypropylene fibers improve the spalling behavior of in-situ concrete?" Cement and Concrete Research **36**(5): 929-942.